Primate superior colliculus is causally engaged in abstract higher-order cognition

Barbara Peysakhovich, Ou Zhu, Stephanie M Tetrick, Vinay Shirhatti, Alessandra A Silva, Sihai Li, Guilhem Ibos, Matthew C Rosen, W. Jeffrey Johnston, David J Freedman

nature neuroscience

Article

https://doi.org/10.1038/s41593-024-01744-x

Primate superior colliculus is causally engaged in abstract higher-order cognition

Received: 14 May 2023

Accepted: 31 July 2024

Published online: 19 September 2024

Check for updates

Barbara Peysakhovich[1], Ou Zhu[1], Stephanie M. Tetrick[1], Vinay Shirhatti[1], Alessandra A. Silva[1], Sihai Li[1], Guilhem Ibos[1,2], Matthew C. Rosen[1], W. Jeffrey Johnston[1] & David J. Freedman[1,3]

The superior colliculus is an evolutionarily conserved midbrain region that is thought to mediate spatial orienting, including saccadic eye movements and covert spatial attention. Here, we reveal a role for the superior colliculus in higher-order cognition, independent of its role in spatial orienting. We trained rhesus macaques to perform an abstract visual categorization task that involved neither instructed eye movements nor differences in covert attention. We compared neural activity in the superior colliculus and the posterior parietal cortex, a region previously shown to causally contribute to abstract category decisions. The superior colliculus exhibits robust encoding of learned visual categories, which is stronger than in the posterior parietal cortex and arises at a similar latency in the two areas. Moreover, inactivation of the superior colliculus markedly impaired animals' category decisions. These results demonstrate that the primate superior colliculus mediates abstract, higher-order cognitive processes that have traditionally been attributed to the neocortex.

Categorization is a fundamental cognitive process by which the brain assigns stimuli to behaviorally meaningful groups. Investigations of visual categorization in primates have identified a hierarchy of cortical areas that transform visual feature encoding into abstract category representations[1]. However, categorization behaviors are ubiquitous across diverse animal species, even those without a neocortex, motivating the possibility that subcortical regions may contribute to abstract cognition in primates.

One candidate structure is the superior colliculus (SC), a brainstem region that is evolutionarily conserved across all vertebrate species[2]. The SC has long been known to play a crucial role in directing orienting movements of the eyes and head. Although traditionally thought to implement reflexive motor actions via inputs from upstream brain areas[3–12], the SC is also involved in overt and covert spatial target selection during a wide range of behavioral tasks[13–30]. However, it is unknown whether the SC is also involved in mediating cognitively demanding tasks that do not manipulate spatial orienting, covert attention or target selection.

Here, we investigated whether the primate SC is more generally involved in abstract cognition. We trained monkeys to perform an abstract visual categorization task that dissociates sensory, cognitive and motor components, and compared neuronal activity in the SC and the lateral intraparietal area (LIP), a cortical region in the posterior parietal cortex that is anatomically interconnected with the SC[31–36] and known to causally contribute to category processing[37,38]. Importantly, the categorization task required the monkeys to maintain central gaze fixation during all task epochs, and the animals reported their decisions with a manual response and not an eye movement. We also reversibly inactivated the SC to assess its causal contribution to category decisions. We show that the SC exhibits robust, short-latency encoding of abstract categories and that inactivation of the SC markedly impairs animals' categorization task performance. These results indicate that the primate SC plays an unexpected key role in higher-order cognition, independent of its role in spatial orienting. In addition, we show that category- and saccade-related signals are encoded in near-orthogonal population subspaces in the SC, providing an explanation for how a motor structure such as the SC can be recruited to participate in cognitive behaviors without interfering with its well-known motor functions.

[1]Department of Neurobiology, The University of Chicago, Chicago, IL, USA. [2]Institut de Neurosciences de la Timone, Aix-Marseille Université, CNRS, Marseille, France. [3]Neuroscience Institute, University of Chicago, Chicago, IL, USA. e-mail: dfreedman@uchicago.edu

https://doi.org/10.1038/s41593-024-01744-x

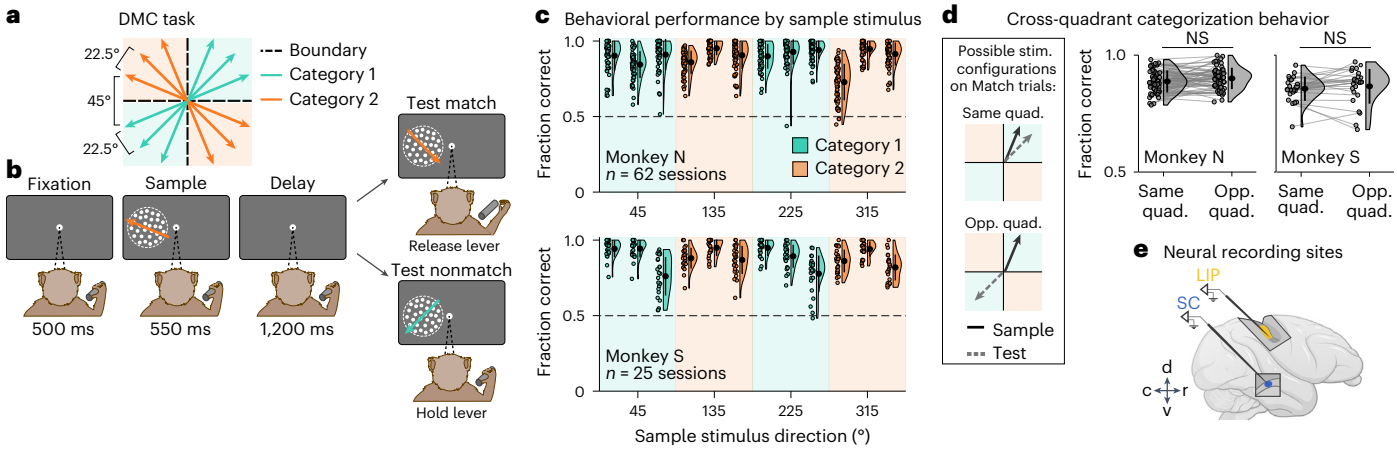

Fig. 1 | Monkeys learn to categorize motion stimuli based on an arbitrary category rule. a, Stimulus geometry of the two-boundary DMC task. Twelve directions of motion (depicted by arrows) are grouped into two categories based on two orthogonal category boundaries (dashed lines), such that directions that are 180° apart belong to the same category. Directions within the same quadrant are 22.5° apart, and near-boundary directions are 22.5° from the boundary. **b**, Trial structure of the DMC task. Monkeys were required to maintain gaze within a small window centered on a central fixation cue during fixation, sample, delay and test periods and report their decisions with a manual response (holding or releasing a lever). **c**, Behavioral performance across recording sessions for each of the 12 sample stimulus directions for Monkey N (top) and Monkey S (bottom). Black circles indicate mean and vertical black bars indicate s.d. Horizontal dashed line indicates chance performance. **d**, Behavioral performance across sessions on Match trials in which the sample and test stimuli were in the same or opposite quadrants. Black circles indicate mean and vertical black bars indicate s.d. There was no significant difference in mean performance on trials in which sample and test stimuli were in the same or different quadrants (Monkey N: $n = 62$ sessions, Same quad. = 88.2 ± 4.6%, Opp. quad. = 86.9 ± 4.7%, $P = 0.130$; Monkey S: $n = 25$ sessions, Same quad. = 84.9 ± 7.4%, Opp. quad. = 83.8 ± 5.2%, $P = 0.583$, two-tailed permutation test). **e**, Schematic of neural recording locations in LIP and the SC. d, dorsal; c, caudal; v, ventral; r, rostral; NS, not significant; Opp. quad., opposite quadrant; same quad., same quadrant.

Results

Behavior

Two monkeys performed a delayed match-to-category (DMC) task in which they grouped 360° of motion directions into two categories based on a learned arbitrary category rule. The categories were defined by two perpendicular boundaries that produced four 90°-wide quadrants (Fig. 1a). To disambiguate neuronal encoding of direction versus category, opposite quadrants were assigned to the same category, such that motion directions that are 180° apart belonged to the same category while nearby directions were often in different categories. On each trial, monkeys viewed sample and test motion stimuli separated by a 1.2-s delay (Fig. 1b) and received a fluid reward for releasing a manual touch bar when the category of the test matched the sample. If the test category was a nonmatch, the monkeys were shown a second test stimulus that always matched the sample category (and required a manual response). Monkeys were required to maintain gaze fixation throughout the trial (Methods). The monkeys' category decisions were abstract because the two categories were defined by the learned arbitrary boundaries, and because they were not explicitly and rigidly linked to different motor actions.

Both monkeys performed the DMC task with >85% mean accuracy during neural recordings (Monkey N: 89.4 ± 3.4%, Monkey S: 88.2 ± 3.3%; Fig. 1c), with equivalent accuracy between LIP and SC sessions (Monkey N: $P = 0.095$, Monkey S: $P = 0.234$, permutation test; Extended Data Fig. 1). Monkeys performed similarly on Match trials in which sample and test stimuli were in the same versus opposite quadrants (Monkey N: $P = 0.130$, Monkey S: $P = 0.583$, permutation test; Fig. 1d).

Robust encoding of sample category in the SC

We recorded neural activity during the DMC task in the SC (Monkey N: 362 neurons, Monkey S: 243 neurons) and LIP (Monkey N: 228 neurons, Monkey S: 327 neurons) (Fig. 1e), a posterior parietal region that has been suggested by our group to be the cortical nexus of category computation. Our past work has shown that LIP has shorter-latency category encoding compared with other cortical areas such as prefrontal cortex and medial superior temporal area[39–42], and reversible inactivation of LIP impairs monkeys' categorization behavior[37,38].

LIP neuronal activity often showed binary-like category selectivity during the sample and delay periods, with distinct activity for directions in different categories and similar activity for directions in the same category (Fig. 2a), consistent with previous categorization studies that used a simpler linear boundary[38–45]. In our task, LIP category selectivity extended even to stimuli in opposite quadrants that belong to the same category. Remarkably, SC neurons also showed strong category selectivity during the sample, delay and test periods of the task (Fig. 2b).

We quantified category tuning in individual neurons using a receiver operating characteristic (ROC)-based category tuning index (rCTI), which compares neuronal discrimination between directions in the same versus different categories (Supplementary Fig. 1 and Methods). Positive rCTI values indicate larger differences in firing rates between directions in different versus the same category (that is, category tuning). The bottom panels of Fig. 2a,b show the time course of rCTI for the single-neuron examples in the corresponding top panels, and Fig. 2c,d shows rCTI values for all LIP and SC neurons. Overall, 70.3% of LIP neurons (Monkey N: 81.1%, Monkey S: 62.7%) and 59.5% of SC neurons (Monkey N: 63.5%, Monkey S: 53.5%) were significantly category-tuned based on rCTI.

In LIP and SC, the mean rCTI across neurons was significantly elevated at nearly every timepoint following sample onset (Fig. 2e, yellow and blue symbols above panel), with greater rCTI values observed in SC than LIP throughout much of the trial (Fig. 2e, black symbols above panel). Moreover, elevated mean rCTI values during the sample period occurred earlier in SC than LIP (SC: 160 ms, LIP: 245 ms; $P = 0.002$, two-tailed permutation test). To compare the onset of category selectivity between LIP and SC, we restricted analyses to neurons that were category-tuned during the 550 ms after sample onset (LIP: $n = 131$ neurons, SC: $n = 133$). Among these early-onset tuned neurons, SC had lower median latency than LIP (Fig. 2f, left; LIP: 330 ± 105 ms, SC: 270 ± 90; $P = 0.016$, two-tailed permutation test), and latency distributions were significantly different between the two areas (Fig. 2f, right;

https://doi.org/10.1038/s41593-024-01744-x

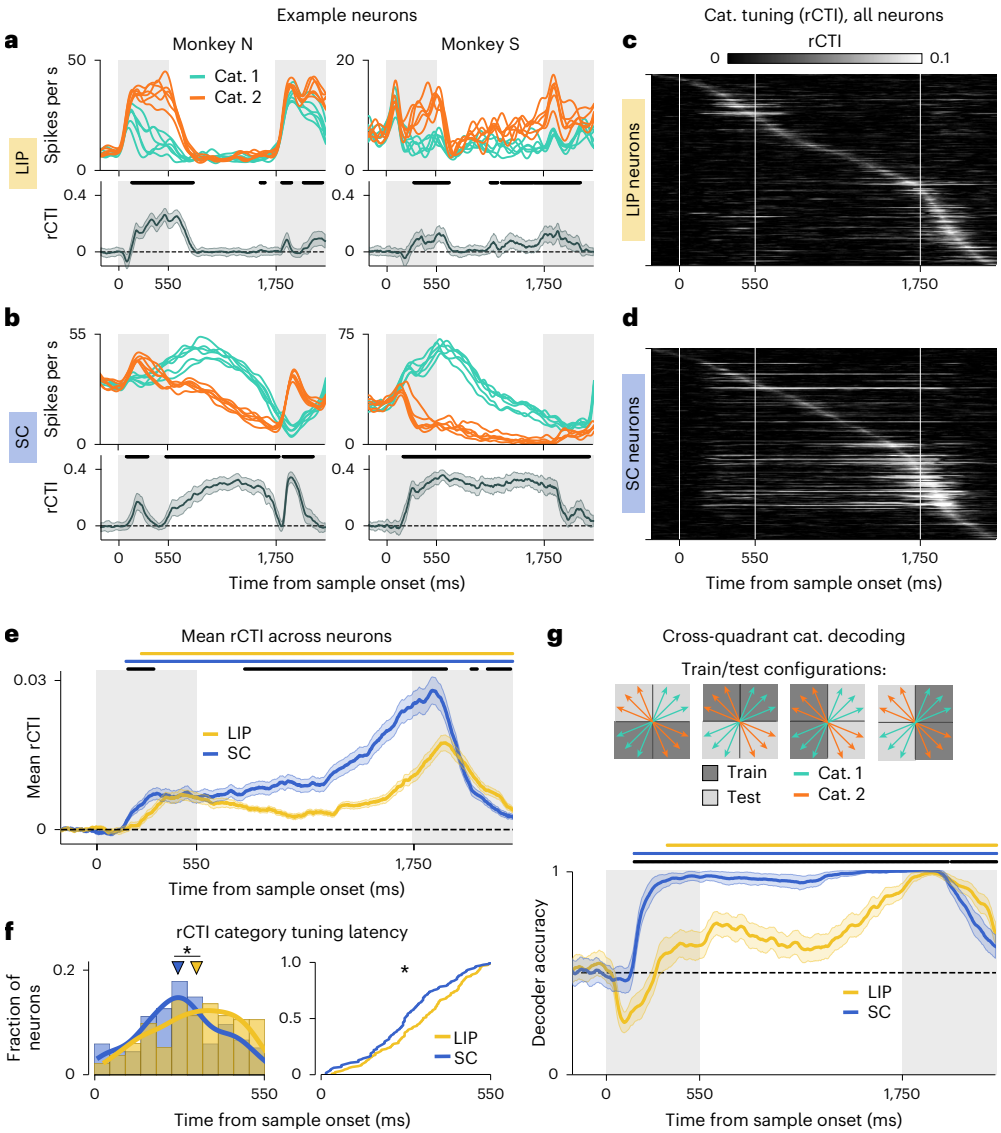

Fig. 2 | Neural activity in the SC contains reliable and short-latency information about stimulus category. a, Top: peristimulus time histograms of example category-tuned LIP neurons. Bottom: rCTI across time in trial for the two example LIP neurons in **a**. Line and shading indicate mean and s.d., computed via resampling of trials. Black bars at the top of the plots indicate timepoints at which rCTI is significantly above chance. **b**, Same as **a**, but for SC. **c**, rCTI across time in trial for the two example LIP neurons in **a**. **c**, Matrix of rCTI values for all LIP and SC neurons, where each row shows a single neuron's rCTI as a function of time in the trial. **d**, Same as **c**, but for SC. **e**, Time course of mean rCTI across LIP and SC neurons. Shading indicates s.e.m. **f**, Latency of category selectivity in neurons that are category-tuned during the sample epoch (0–550 ms from sample onset; LIP: $n = 131$ neurons, SC: $n = 133$ neurons). Left: distribution of category selectivity latency. Triangular markers indicate median latency (LIP: 330 ± 105 ms, SC: 270 ± 90; $P = 0.016$, two-tailed permutation test). Right: empirical cumulative distribution functions of latency values in LIP and SC neurons (two-sample Kolmogorov–Smirnov test, $D = 0.195$, $P = 0.011$). **g**, Top: schematic of cross-quadrant sample category classifiers, which are trained on trials from two quadrants (dark gray) and validated on trials from the remaining two quadrants (light gray). Bottom: time course of mean accuracy of cross-quadrant category classifiers for LIP and SC populations. Horizontal dashed line indicates the chance accuracy level (0.5). Shading indicates s.d. In **e** and **g**, colored symbols above the panel indicate timepoints at which values significantly exceed chance in each brain area, and black bars above the panel indicate timepoints at which there is a significant difference between brain areas ($P < 0.05$, two-tailed permutation tests). *$P < 0.05$. Cat., category.

two-sample Kolmogorov–Smirnov test, $D = 0.195$, $P = 0.011$). Additionally, we observed significantly longer durations of persistent category selectivity in SC than LIP neurons (Supplementary Fig. 2 and Methods).

These differences in strength and timing of category tuning cannot be explained by differences in direction tuning between areas (Supplementary Fig. 3); when we restricted analyses to direction-untuned neurons (LIP: $n = 399$, SC: $n = 498$; Methods), we again observed shorter-latency category selectivity in SC compared with LIP based on mean rCTI across neurons (SC: 160 ms, LIP: 225 ms, $P = 0.004$, two-tailed permutation test) and median category tuning latency during the sample period (LIP: 330 ± 105 ms, $n = 111$ neurons, SC: 265 ± 80, $n = 107$, $P = 0.005$, two-tailed permutation test; Kolmogorov–Smirnov test: $D = 0.225$, $P = 0.007$). We also observed equivalent results when we artificially matched mean firing rates of SC and LIP neurons at each analysis time step by randomly removing spikes from SC neurons (Methods and Supplementary Fig. 4).

We quantified the strength and timing of category encoding in LIP and SC populations using support vector machine (SVM) classifiers. We evaluated category encoding in a direction-independent manner by training the classifiers on trials from two quadrants (one per category) and validating them on the remaining two quadrants (Fig. 2g, top). If the neural populations robustly encode category in a binary-like format,

the classifier will generalize between the two quadrants of the same category. This approach also prevents bell-shaped direction tuning from contributing to category decoding by decorrelating direction and category between the sample and test sets; note that this procedure produces below-chance classifier performance if the population shows strong direction tuning.

In SC, category classifier accuracy rapidly increased within ~170 ms of sample onset and remained at almost 100% throughout the rest of the trial (Fig. 2g, bottom). In LIP, category classifier accuracy was below chance shortly after sample onset, consistent with bell-shaped direction tuning in LIP during the early sample (Supplementary Fig. 3). Sample category could be decoded more reliably from SC than LIP throughout the sample, delay and early test phases of the task (Fig. 2g, bottom, black symbols above panel), indicating stronger population category encoding in SC than LIP. These results were similar in the two animals (Supplementary Fig. 5).

Category encoding in SC is not explained by eye movements

Given the well-established role of SC in directing gaze[3–12], one explanation for category selectivity in SC is that it could be a result of distinct patterns of microsaccades during different conditions of the DMC task. Interestingly, we indeed observed that the monkeys produced idiosyncratic, category-specific eye movements (within the allowed fixation window) that were highly stereotyped across sessions (Supplementary Fig. 6). However, these category-specific eye movements occurred only during the memory delay in Monkey N and primarily during the delay in Monkey S, indicating that the monkeys' eye movements reflect the contents of working memory, consistent with previous results in monkeys performing a delayed matching task[46]. Notably, the category-specific eye movements were not observed in the early-sample period when neuronal category selectivity emerged in SC (and LIP). We compared the time course of SC's neuronal category selectivity and the time course of category-specific eye positions. These two time courses were highly decoupled in time (Supplementary Fig. 7a), with category selectivity preceding category-specific eye position by hundreds of milliseconds (Monkey N: neural decoder = 175 ms, eye decoder = 1,075 ms; Monkey S: neural decoder = 170 ms, eye decoder = 865 ms). We next built linear encoding models[47] to determine whether neuronal firing rates (across trials and time within trial) are better predicted by category or eye movements (Methods). For a majority of SC neurons, firing rates during the DMC task were better predicted by the stimulus than by eye movements (Supplementary Fig. 7b). These results indicate that SC category selectivity cannot be accounted for by category-specific eye movements during the DMC task, and raise the possibility that the eye movements may instead be a consequence of the presence of category selectivity in the SC.

Preferential encoding of category in visual SC neurons

The SC is a core stage of oculomotor processing and contains diverse neuronal response types based on firing rate modulation to visual, visuomotor and motor aspects of visually guided saccade (VGS) and memory-guided saccade (MGS) tasks. We sought to understand whether SC category encoding was more prevalent among neurons with particular patterns of visual or motor selectivity. In each DMC recording session, monkeys also performed the MGS task (Supplementary Fig. 8a,b), allowing us to compare neuronal activity from the same neurons during the two tasks. We analyzed activity from 424 SC neurons (Monkey N: 259, Monkey S: 165) with stable recordings during both DMC and MGS tasks. Examples of SC activity during the MGS task are shown in Supplementary Fig. 8c,d.

The short-latency category encoding in SC raises the possibility that it plays a direct role in the rapid bottom-up categorization of incoming visual stimuli (that is, the transformation of direction to category tuning). One piece of evidence that would support such a role is if the category signal first emerges in visually responsive neurons whose receptive fields match the position of the DMC stimuli (Extended Data Fig. 2a). We compared rCTI values between three groups of SC neurons (Methods): (1) those that are visually responsive during the MGS task to stimuli at locations that overlap with the stimulus in the DMC task (Vis neurons; $n = 127$); (2) neurons that are visually unresponsive at the DMC stimulus location but visually responsive at other locations (Vis-other; $n = 167$); and (3) visually unresponsive neurons (Non-vis; $n = 130$). Examples of these three classes of neurons are shown in Extended Data Fig. 2b.

Category selectivity emerged earlier in Vis neurons than in Vis-other neurons (Vis: 155 ms, Vis-other: 205 ms; $P = 0.021$, permutation test) and Non-vis neurons (Non-vis: 634 ms; $P < 0.001$, two-tailed permutation test; Extended Data Fig. 2c), and mean rCTI was significantly higher in Vis neurons compared with the other two groups throughout much of the trial (Extended Data Fig. 2c, black symbols above panel). Additionally, median category selectivity latency during the sample period was lower in Vis neurons compared with Vis-other neurons, even when we artificially matched firing rates between the two groups as for the earlier analysis of LIP versus SC latency (Extended Data Fig. 2d, left; Vis: 228 ± 75 ms, $n = 48$; Vis-other: 330 ± 95, $n = 35$; $P = 0.001$, two-tailed permutation test), and there was a significant difference in the latency distributions between Vis and Vis-other (Extended Data Fig. 2d, right; two-sample Kolmogorov–Smirnov test, $D = 0.407$, $P = 0.002$).

Category encoding in SC and LIP is dependent on task context

We next investigated whether category encoding in LIP or SC depended on the context in which the monkeys viewed sample motion stimuli. It is possible that the animals' extensive training on the DMC task could have led to automatized processing of motion category in SC or LIP even when stimuli were shown outside of the DMC task context. We tested this possibility by comparing neuronal responses to motion stimuli during interleaved blocks of DMC task trials and passive viewing trials in which the same motion stimuli were shown (Methods). Neuronal category encoding in both SC and LIP was largely absent during passive viewing trials (Supplementary Fig. 9), indicating that category selectivity is highly task-dependent and that neural populations in LIP and SC can flexibly route sensory input based on current behavioral demands.

Orthogonal encoding of saccades and category in the SC

How is it that a core oculomotor structure such as the SC can be strongly modulated by stimulus category (or visual information in general) without producing task-interfering saccades, given that injection of even a small amount of electrical current into intermediate and deep layers of the SC can reliably generate large-amplitude eye movements[6,7]? One explanation is that independent populations of SC neurons might participate in saccade and category encoding. Thus, we quantified the overlap in neural populations that are category-selective during the DMC task and saccade direction-selective during the MGS task (Methods). We observed substantial overlap in the population of SC neurons that are category- and saccade-selective (Fig. 3a), indicating that category and saccade encoding are not segregated to different SC populations.

We hypothesized that the structure of population activity in the SC is organized to maintain approximately orthogonal neural representations during category processing and saccade planning, such that projection of category-related neural activity onto the saccade-encoding neural axis produces minimal interference with neural encoding of eye movements (Fig. 3b). To investigate this idea, we characterized the alignment between neural activity from the DMC task (150–350 ms after sample onset) and the MGS task (−200–0 ms before saccade onset). To visualize their alignment, we used targeted dimensionality reduction[48] to identify two MGS condition-related neural axes (sin and cos of the position of the targets) and a DMC category axis. The DMC

https://doi.org/10.1038/s41593-024-01744-x

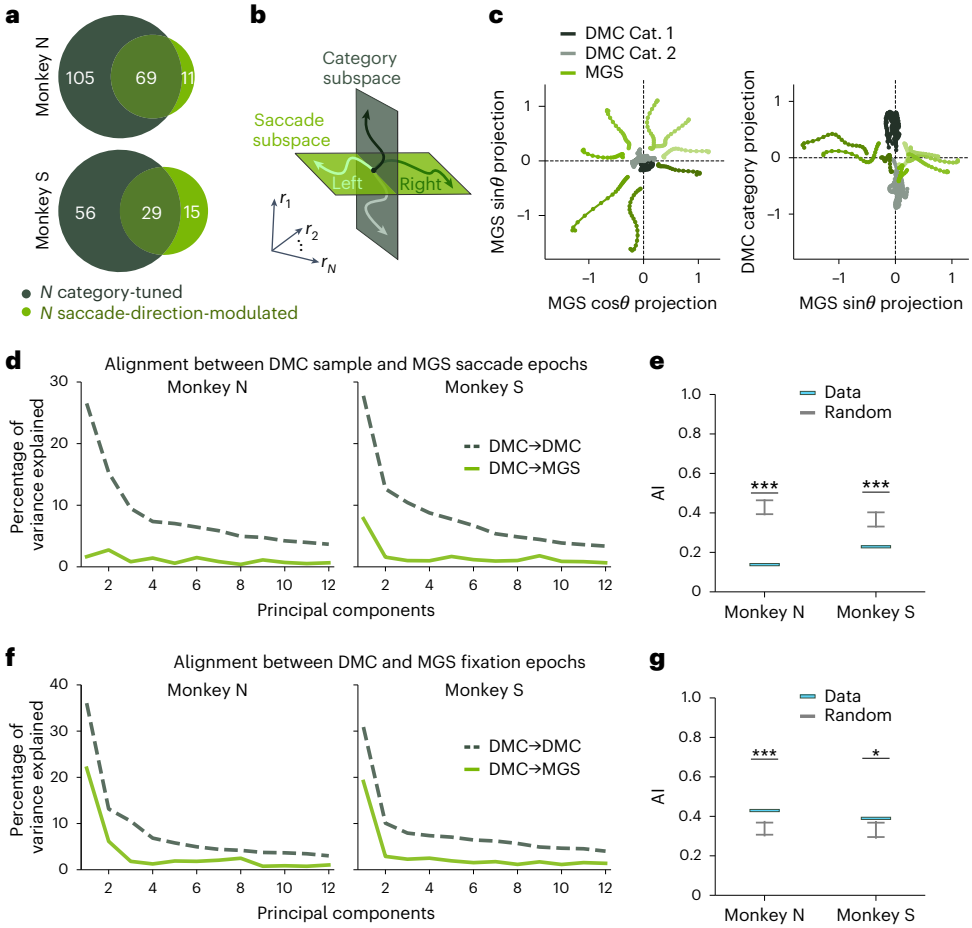

Fig. 3 | Orthogonal population-level encoding of saccade and category in the SC. a, Venn diagrams showing the overlap of neurons that are category-tuned during the DMC task (dark green) and neurons that are saccade-direction-modulated during the MGS task (light green; Methods). **b**, Schematic of the hypothesized orthogonal saccade and category activity subspaces. **c**, Left: magnitude of the projections of: (1) the sine and cosine values from MGS data (green); and (2) the two categories from DMC data (gray and black) from Monkey N onto the two MGS neural axes identified through targeted dimensionality reduction (TDR). Right: projection of the same MGS and DMC data from Monkey N onto one of the MGS TDR axes and the DMC category axis. **d**, The percentage of variance of DMC sample period data explained when projected onto its own top 12 PCs (dashed dark green line) or onto the top 12 PCs defined by activity during the peri-saccade period (−200 to 0 ms from saccade onset) of the MGS task (solid light-green line). **e**, AI between the DMC sample epoch data and MGS peri-saccade data. The AI, which is the ratio of the sums of the two traces shown in **d**, equals 1 when two subspaces are perfectly aligned and equals 0 when two subspaces are perfectly orthogonal. Blue, alignment indices for the real data. Gray, 95% confidence intervals of alignment indices between pairs of random vector projections from data (Methods). For both monkeys, the real data are significantly more orthogonal than expected by chance (Monkey N: AI = 0.131, $n = 258$ neurons; Money S: AI = 0.205, $n = 165$ neurons), all $P < 0.001$, two-tailed randomization test. **f**,**g**, same as **d** (**f**) and **e** (**g**) but for the fixation epochs (−500 to 0 ms relative to stimulus onset) for the DMC and MGS tasks. The data are significantly more aligned than expected by chance (Monkey N: AI = 0.429, $n = 259$ neurons, $P < 0.001$; Money S: AI = 0.390, $n = 165$ neurons, $P = 0.007$, two-tailed randomization test). $^*P < 0.05$, $^{***}P < 0.001$.

data had a small projection onto the MGS axes, as did the MGS data onto the category axis (Fig. 3c), indicating substantial misalignment between category and saccadic encoding.

To quantify the alignment between neural activity during the MGS and DMC tasks, we used the subspace variance alignment analysis introduced previously[49]. This approach compares the percentage of DMC data variance explained when the DMC data are projected onto DMC-defined versus MGS-defined principal components (PCs) and produces an alignment index (AI) value that ranges from 0 (indicating total orthogonality between two subspaces) to 1 (indicating perfect alignment). To determine statistical significance, we compared the AI computed from the data with a null distribution of AI values between subspaces drawn from a random space that shares a covariance structure with the real data (Methods).

In both monkeys, the category and saccade subspaces were near-orthogonal; projection of the DMC data onto the first 12 MGS PCs captured minimal DMC data variance (Fig. 3d), and the resulting AI was closer to 0 than expected by chance (Fig. 3e; Monkey N: AI = 0.131, $P < 0.001$, $n = 258$ neurons; Money S: AI = 0.205, $P < 0.001$, $n = 165$ neurons). This misalignment did not depend on the number of PCs included in the analysis; the DMC and MGS data were significantly misaligned when the analysis was repeated using different numbers of included PCs (Supplementary Fig. 10). This result is also unlikely to be due to neural fluctuations over time in the session; in both monkeys, DMC activity from the beginning of the sessions was closely aligned to DMC activity from the end of the sessions (Extended Data Fig. 3a), and alignment to MGS activity was similarly low for DMC activity from the beginning versus end of the sessions (Extended Data Fig. 3b). To determine whether this misalignment between category and saccade subspaces may be due to general differences in behavioral state in the two task contexts, we quantified the alignment between the baseline neural activity during the fixation epochs (from −500 to 0 ms relative to stimulus onset) for the two tasks. During this baseline period, the task demands (that is, maintaining fixation) are shared between the two tasks, but the overall behavioral context is different. In both monkeys, fixation epoch activity during the DMC and MGS tasks was more aligned

than expected by chance (Fig. 3f,g; Monkey N: AI = 0.429, $P < 0.001$, $n = 259$ neurons; Money S: AI = 0.390, $P = 0.007$, $n = 165$ neurons), indicating that the misalignment between category and saccade subspaces cannot be explained by differences in behavioral state between tasks, and suggesting that the SC may selectively use an orthogonal-coding strategy to minimize motor interference.

Together, these results suggest a mechanism by which neural populations in the SC can multiplex motor signals and the higher-order cognitive signals that we report here. These results also provide a possible explanation for the stereotyped, category-specific microsaccades that emerge several hundred microseconds after neural category selectivity onset during the DMC task (Supplementary Figs. 6 and 7); these category-specific eye movements may reflect 'leak' from the category subspace to the saccade subspace. During learning of the DMC task, the SC network may arrive at a particular geometry of population activity that is sufficiently (although not perfectly) orthogonal to the saccade subspace, such that any resulting eye movements are within the behavioral constraints of the task (that is, fall within the allowed fixation window).

Impaired category task performance during SC inactivation

We sought to determine whether neuronal category encoding in the SC plays a causal role in the DMC task by infusing muscimol, a $GABA_A$ agonist, to reversibly inactivate the SC before task performance (Fig. 4a and Supplementary Table 1). We compared monkeys' behavior during SC inactivation with behavior during control blocks collected before injection on the same day. SC inactivation is known to cause a reduction of velocity for saccades toward targets contralateral to the inactivated hemisphere[10–12]. To verify inactivation efficacy, we compared saccade velocities for an MGS (Monkey N) or VGS (Monkey S) task before versus after inactivation (Fig. 4b). Although both monkeys were able to successfully perform the saccade task following injection, we observed a reduction in saccade velocity to targets in the inactivated hemifield (Fig. 4c), both for data combined across all sessions (Monkey N: control = 418 ± 90° s^{-1}, treatment = 249 ± 51° s^{-1}, $P < 0.001$; Monkey S: control = 420 ± 106° s^{-1}, treatment = 193 ± 92° s^{-1}, $P < 0.001$, two-tailed permutation test) and for each individual session (Supplementary Table 2). This effect was absent for sham control sessions (saline injection) (Supplementary Table 2; Monkey N: control = 432 ± 90° s^{-1}, treatment = 438 ± 95° s^{-1}, $P = 0.673$; Monkey S: control = 415 ± 84° s^{-1}, treatment = 413 ± 87° s^{-1}, $P = 0.848$, two-tailed permutation test).

Both monkeys showed a marked impairment in DMC task performance after muscimol injection (Fig. 4d,e), with a reduction in DMC accuracy on every muscimol infusion session, and no change on saline sessions (Supplementary Table 3). These results are consistent with SC being causally involved in DMC task performance. Notably, the DMC task deficits that we observed during SC inactivation were substantially larger than those previously reported during LIP inactivation during a DMC task[38] (Fig. 4f). The larger effect of SC versus LIP inactivation on DMC performance cannot be explained by differences in muscimol concentration (SC = 5 μg $μl^{-1}$, LIP = 8 μg $μl^{-1}$) or infusion volume (SC = 0.25–0.33 μl, LIP = 6–9 μl) between experiments. Although these experiments were performed in different monkeys, used slightly different versions of the DMC task (for example, different category boundary structures) and used different muscimol infusion protocols (Methods), this comparison suggests that the SC may have an even more critical role in mediating the DMC task than LIP.

SC inactivation equally affected performance on trials in which the sample stimulus was from Category 1 versus Category 2, as well as on Match trials in which the Sample and Test stimuli were in the same versus opposite quadrants (Extended Data Fig. 4). However, both monkeys showed a bias in inactivation effects between Match and Nonmatch trials (Extended Data Fig. 4c,d). Monkey N had a significantly larger impairment for Match trials (Match = −59.1 ± 18.8%, Nonmatch = 2.3 ± 2.9%, $U = 0$, $P = 0.002$, Wilcoxon rank-sum test), while Monkey S had a significantly larger impairment for Nonmatch trials (Match = −17.6 ± 3.6, Nonmatch = −28.4 ± 4.6, $U = 1$, $P = 0.004$). Investigation of Monkey N's behavior revealed that during many inactivation sessions, he held the touch bar throughout the Test 1 epoch for all trials and released the lever during the Test 2 stimulus (which only appeared during Nonmatch trials). Therefore, after SC inactivation, his performance was close to 0% for Match trials and was close to 100% for Nonmatch trials. This may reflect a behavioral strategy to optimize reward and minimize effort; he may have adopted this strategy to receive reward on 50% of the trials if he had difficulty interpreting or remembering the stimulus category following SC inactivation.

The behavioral impairment on the DMC task during SC inactivation is unlikely to be largely due to deficits in low-level visual processing of stimuli presented in the inactivated hemifield. The DMC deficit is not purely an attentional/hemispatial neglect-like impairment, as the monkeys are still able to perceive and respond to stimuli presented in the inactivated hemifield during the MGS task, and still attempt the DMC task and respond at appropriate times in the trial (that is, release the lever only during the test epochs). The DMC deficit is also unlikely due to an impairment in sensory processing of motion stimuli, as previous studies using similar experimental protocols have shown that SC inactivation produces minimal impairments in direction discrimination of high-coherence motion stimuli such as those in our DMC task[28].

We note that our experimental design cannot isolate the precise nature of the deficit caused by SC inactivation, as the DMC task requires several complex computations, including transforming sample direction into category, maintenance of category information in working memory, computation of the test category and comparing sample and test categories. Our recordings identified encoding of each of these task variables in SC, so that the behavioral deficits observed during SC inactivation may result from interfering in any combination of these factors. Future targeted experiments can more precisely characterize the nature of the deficit(s) caused by SC inactivation. Despite this limitation, our study reveals that the functions of primate SC extend well beyond those ascribed to it by previous studies, which had, to our knowledge, never tested SC's role in cognitive tasks that involve neither eye movements, target selection, nor explicit modulation of covert spatial attention.

Shorter-latency match versus nonmatch encoding in SC than LIP

Finally, we were interested in whether there were differences between LIP and SC encoding during the test period when the monkey had to decide whether the category of the currently visible test stimulus matched the sample stimulus shown earlier in the trial. We applied SVM classifiers to activity during the first test period on Match and Nonmatch trials and computed latency values for each classifier run as the first time bin the classifier value exceeded 75% for five consecutive time bins. When applied to pooled pseudopopulations containing all neurons from both monkeys (Fig. 5a), encoding of Match versus Nonmatch arose with a shorter mean latency in SC (135 ± 6 ms) than LIP (176 ± 18 ms) (bootstrap, $P < 0.001$), suggesting that SC is preferentially involved in the monkeys' match versus nonmatch decisions compared with LIP. This analysis revealed similar results when applied separately for Monkey N (SC latency = 136 ± 6 ms, LIP latency = 168 ± 18 ms, $P < 0.001$) and Monkey S (SC latency = 162 ± 9 ms, LIP latency = 230 ± 13 ms, $P < 0.001$) (Fig. 5b).

Discussion

We demonstrate that the primate SC is involved in abstract visual categorization, a cognitive function that was previously thought to be mediated by cortical association areas. Our results indicate that the role of the primate SC extends beyond sensorimotor functions and spatial orienting to abstract, higher-order cognitive processing, even in tasks that do not involve reporting decisions with saccades.

https://doi.org/10.1038/s41593-024-01744-x

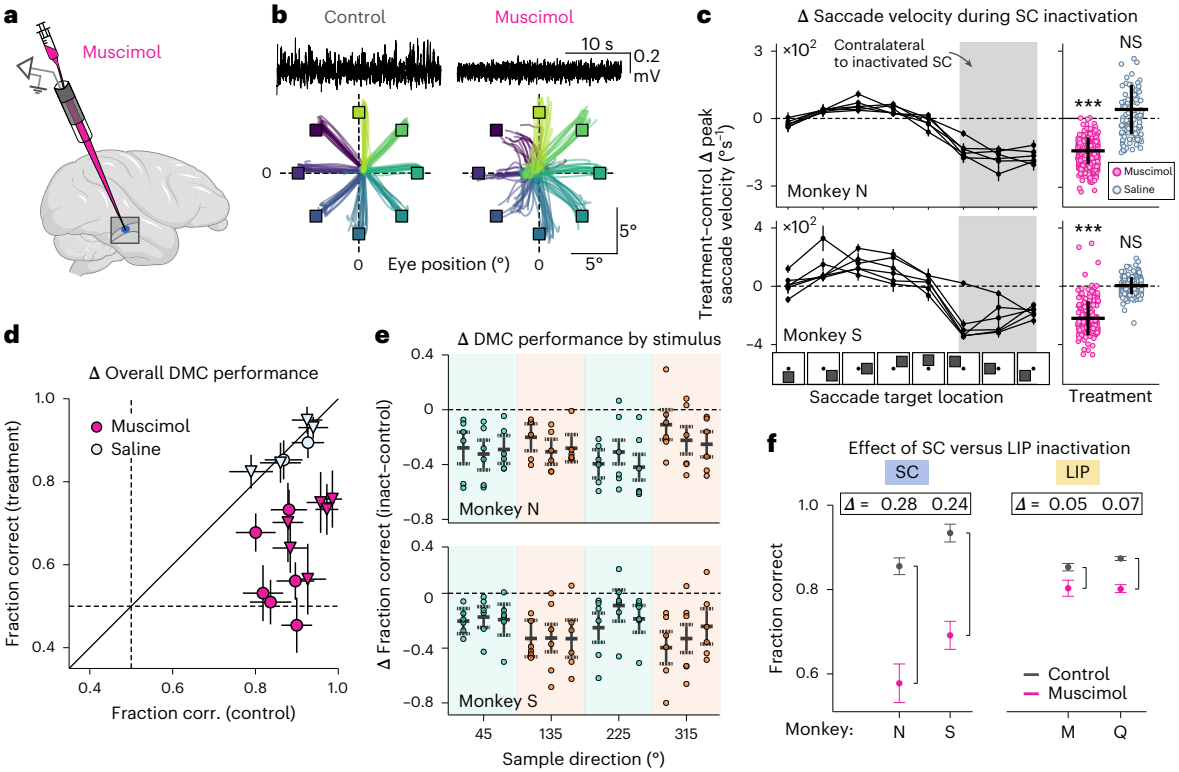

Fig. 4 | SC is causally involved in categorization task performance. a, We performed reversible unilateral inactivation of the SC by infusing muscimol, a $GABA_A$ agonist, using a custom 16-channel recording probe with a fluid delivery channel. **b**, Top: following injection of muscimol, spiking activity markedly decreased in the surrounding tissue. Bottom: trajectories of eye movements in Monkey S during the VGS task for an example session before (left) and after (right) muscimol injection. Individual traces represent eye gaze trajectories for individual trials and are color-coded by condition. Small colored squares indicate the position of saccade targets for different conditions. **c**, Left: changes in peak saccade velocity during the MGS/VGS task before and after SC inactivation at each of the eight stimulus locations used in the task. Traces indicate mean ± s.e.m. Gray background shading indicates conditions in which the target location was in the inactivated hemifield. Right: change in peak saccade velocity for trials (across all sessions) in which the target was in the inactivated hemifield for muscimol (magenta) and saline (blue) injection sessions. In both monkeys, we observed a significant reduction in peak velocity for muscimol sessions (Monkey N: $n = 654$ trials, $-166 \pm 55°\ s^{-1}$, $P < 0.001$; Monkey S: $n = 497$ trials, $-219 \pm 117°\ s^{-1}$, $P < 0.001$, two-tailed permutation test) and no change in peak velocity for saline sessions (Monkey N: $n = 174$ trials, $4 \pm 101°\ s^{-1}$, $P = 0.651$; Monkey S: $n = 400$ trials, $5 \pm 59°\ s^{-1}$, $P = 0.881$, two-tailed permutation test). Horizontal black bars indicate mean of distributions and vertical black bars indicate s.e.m. For each treatment trial, we quantified the change in peak velocity as the difference in peak velocity on that trial and the mean peak saccade velocity for that trial type from the preceding control block. ***$P < 0.001$. **d**, Overall session accuracy for the DMC task before versus during SC inactivation. Horizontal and vertical dashed lines indicate the chance accuracy level (0.5.) Unfilled, saline injection; filled, muscimol; circles, Monkey N; triangles, Monkey S. Error bars, 95% multinomial confidence intervals for each session. **e**, Mean change in performance on the DMC task for each of the 12 sample motion stimuli during inactivation vs. control, colored by category. Gray bars indicate mean ± s.e.m. **f**, Comparison of the behavioral impairments on the DMC task during SC versus LIP inactivation. Left: behavior performance on the DMC task during control blocks (gray) and SC inactivation blocks (magenta) for Monkey N and Monkey S. Traces show mean accuracy ± s.e.m. for six control sessions and six inactivation sessions in each monkey. Right: behavior performance on the DMC task during control sessions (gray) and LIP inactivation sessions (magenta) for Monkey M and Monkey Q. Traces show mean accuracy ± s.e.m for 12 control/8 inactivation sessions in Monkey M, and 8 control/11 inactivation sessions in Monkey Q. Text indicates the difference in mean accuracy between control and inactivation sessions. LIP data are from ref. 38.

We show that the SC reliably encodes the learned categories of visual stimuli during stimulus presentation, working memory and stimulus comparison periods. Category encoding in the SC arose with a short latency and was stronger than in LIP, a cortical region with the shortest-latency category encoding of all cortical areas previously examined in the DMC task[39,40,42]. During the DMC Test period when the monkeys compared the current Test stimulus with the remembered sample, SC showed stronger and earlier encoding of the monkeys' trial-by-trial decisions. The stronger category- and decision-related encoding in the SC than LIP is especially notable, since LIP had been suggested to be a central node of category processing[1,37–39,42]. Moreover, we show that reversible inactivation of the SC markedly impairs monkeys' DMC task performance, indicating that activity in the SC is causally involved in category task behavior. Although inactivation of the LIP also causes deficits in similar visual categorization tasks[38,50], the impairment that we observed during SC inactivation was substantially larger than those reported during LIP inactivation.

Previous studies that observed cognitive and/or abstract encoding in the primate SC used tasks in which animals either spatially orient to a particular target to indicate their choices[17–23,51–53], or tasks in which animals need to covertly orient to stimuli at distinct locations in different conditions[24–30]. By contrast, in the current study, monkeys did not report their decisions with a saccade or orient attention to different locations for different categories. Thus, it is difficult to account for our results based on differences in covert spatial attention. It is also unlikely that the current results are explained by SC inactivation causing a deficit in motion perception or direction discrimination, as a previous SC inactivation study[28] found that motion direction discrimination was minimally impaired for brief (160-ms) pulses of medium (50%) coherence motion, whereas our study used 100% coherence and a longer presentation duration. Our task also required monkeys to maintain gaze fixation throughout the trial, and category encoding in SC could not be explained by the animals' patterns of eye movements during the task.

https://doi.org/10.1038/s41593-024-01744-x

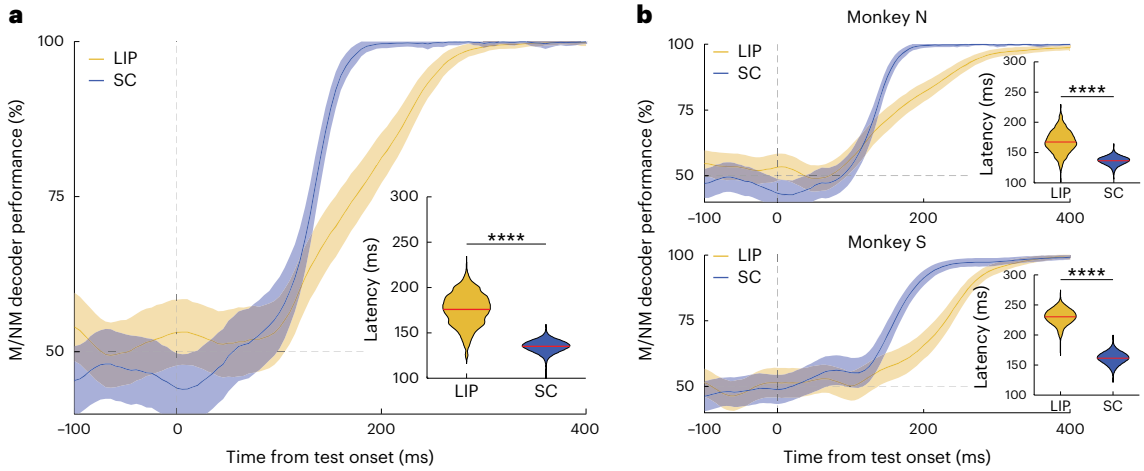

Fig. 5 | SC and LIP activity reflects match versus nonmatch decisions during the test period. Time course of match (M) versus nonmatch (NM) encoding for SC and LIP pseudopopulations was assessed by SVM decoding with a sliding window (width: 30 ms s.d. Gaussian; step size: 5 ms). **a**, Mean accuracy of match versus nonmatch decoding accuracy is shown for a combined pseudopopulation containing all neurons from both monkeys. **b**, Same as **a**, containing neurons from only Monkey N (top) or Monkey S (bottom). For both **a** and **b**, shading indicates s.d., computed via resampling of trials when constructing the pseudopopulation. Horizontal dashed lines indicate the level of decoding expected by chance (50%). Insets show latency distributions and corresponding mean (black line) and median (red line) values for SC and LIP. Statistical significance of bootstrap tests comparing latency distribution means between SC and LIP is indicated in the insets. ****$P < 0.001$.

Our analyses of the alignment of population encoding suggest that the SC population multiplexes category and saccade information by projecting those variables into distinct and near-orthogonal activity subspaces. This can explain how a motor structure such as the SC can simultaneously encode other task variables without interfering with motor encoding or producing task-interfering eye movements, closely related to the mechanism proposed to explain motor planning activity (without motor output) in the primary motor cortex[49]. Even more broadly, this segregation of diverse behavioral functions into separate subspaces could be a general principle of neural coding through which a single neural population can efficiently and robustly encode multiple factors.

We investigated SC during the DMC task because of evidence that cortical areas that are closely involved in oculomotor functions, such as LIP and the frontal eye fields, are also engaged in abstract categorization and flexible decision tasks[54]. Our previous work shows that LIP plays a causal role in abstract categorization[37,38], and that it preferentially encodes motion categories compared both with the middle temporal (MT) and medial superior temporal (MST) visual cortical areas[42,43], and with executive regions such as lateral prefrontal cortex[39]. Anatomical connections between LIP and SC also motivated examining SC[31–36], as well as the similar patterns observed in SC and LIP during saccade-based tasks. We were also inspired by work showing that SC activity reflects higher-order functions such as attention and perceptual decisions (during tasks in which decisions were reported via eye movements or which manipulated covert spatial attention[17–30,51]).

Future directions

The SC is interconnected with a diversity of subcortical and cortical regions[2]. It will be important to investigate the involvement of these different pathways in categorization behavior. Our results also highlight the need to directly and simultaneously compare encoding across the SC–frontal eye field–LIP network to determine their contributions to computing abstract category information from upstream visual cortical regions (for example, MT and MST)[42,43,55], and to understand how communication between these areas supports such decisions.

We speculate that the primate SC is generally involved in abstract visual categorization for a wider range of visual features beyond motion, as cortical areas such as LIP are involved in the categorization of both motion and shapes[56]. It will be interesting to investigate the relative roles of the SC and LIP in motion versus object categorization, as well as the involvement of the SC in nonvisual (for example, auditory) categorization.

Monkeys were trained on the DMC task for hundreds of training sessions over many months. We wonder whether nonspatial task-related encoding in subcortical or motor structures such as the SC emerges only after prolonged training and the resulting expertise on a task. The SC might participate in abstract decision-making even during early stages of learning a task. Alternatively, it is possible that the SC is critical for categorization only after the task becomes well-learned following this extensive training. This would suggest an intriguing relationship between experience level and cortical versus subcortical involvement in higher-order cognition, wherein cognitive functions are first cortically mediated and become subcortically mediated after extensive experience. This idea is supported by a study in mice showing that posterior parietal cortex inactivation impairs categorization performance with newly learned stimuli, but not well-learned stimuli[50]. This idea also aligns with a prominent model of motor learning, according to which early motor skill learning is cortex-dependent but, as behavior becomes increasingly automated, control of the motor skill is gradually transferred to subcortical structures such as the basal ganglia[57]. To determine whether the SC is critical for category learning, or only becomes involved in categorization after extended training, future experiments should compare the effects of SC inactivation on performance during early versus late task learning stages.

Our findings are interesting to consider from an evolutionary perspective and highlight the importance of considering the functions of the SC between mammals and other vertebrates. While previous work in mammalian SC has emphasized its role in simple sensorimotor functions, our work suggests that SC also mediates higher-order behaviors including categorization, working memory and decision-making. It may be advantageous for an area such as the SC, which is close to both sensory input and motor output brain centers, to play such a role to facilitate rapid yet flexible behaviors. The idea that the SC is involved in complex behaviors is especially plausible in nonmammalian vertebrate species, which lack a neocortex and in which the tectum occupies a large fraction of brain volume and is known to play a major role in visual processing. Indeed, studies have found innate spatial encoding of

stimulus size categories in the optic tectum of untrained barn owls[58]. In mammals and primates, this spatial orienting circuit may have evolved to rapidly compute more complex types of information (such as the visual categories described here), while cortical pathways developed to allow for slower but even more sophisticated and flexible processing.

Online content

Any methods, additional references, Nature Portfolio reporting summaries, source data, extended data, supplementary information, acknowledgements, peer review information; details of author contributions and competing interests; and statements of data and code availability are available at https://doi.org/10.1038/s41593-024-01744-x.

References

1. Freedman, D. J. & Assad, J. A. Neuronal mechanisms of visual categorization: an abstract view on decision making. *Annu. Rev. Neurosci.* **39**, 129–147 (2016).
2. Basso, M. A. & May, P. J. Circuits for action and cognition: a view from the superior colliculus. *Annu. Rev. Vis. Sci.* **3**, 197–226 (2017).
3. Apter, J. T. Eye movements following strychninization of the superior colliculus of cats. *J. Neurophysiol.* **9**, 73–86 (1946).
4. Wurtz, R. H. & Goldberg, M. E. Superior colliculus cell responses related to eye movements in awake monkeys. *Science* **171**, 82–84 (1971).
5. Schiller, P. H. & Koerner, F. Discharge characteristics of single units in superior colliculus of the alert rhesus monkey. *J. Neurophysiol.* **34**, 920–936 (1971).
6. Schiller, P. H. & Stryker, M. Single-unit recording and stimulation in superior colliculus of the alert rhesus monkey. *J. Neurophysiol.* **35**, 915–924 (1972).
7. Robinson, D. A. Eye movements evoked by collicular stimulation in the alert monkey. *Vis. Res.* **12**, 1795–1808 (1972).
8. Wurtz, R. H. & Goldberg, M. E. Activity of superior colliculus in behaving monkey. 3. Cells discharging before eye movements. *J. Neurophysiol.* **35**, 575–586 (1972).
9. Sparks, D. L. Functional properties of neurons in the monkey superior colliculus: coupling of neuronal activity and saccade onset. *Brain Res.* **156**, 1–16 (1978).
10. Hikosaka, O. & Wurtz, R. H. Modification of saccadic eye movements by GABA-related substances. I. Effect of muscimol and bicuculline in monkey superior colliculus. *J. Neurophysiol.* **53**, 266–291 (1985).
11. Hikosaka, O. & Wurtz, R. H. Saccadic eye movements following injection of lidocaine into the superior colliculus. *Exp. Brain Res.* **61**, 531–539 (1986).
12. Lee, C., Rohrer, W. H. & Sparks, D. L. Population coding of saccadic eye movements by neurons in the superior colliculus. *Nature* **332**, 357–360 (1988).
13. Basso, M. A. & Wurtz, R. H. Modulation of neuronal activity by target uncertainty. *Nature* **389**, 66–69 (1997).
14. Basso, M. A. & Wurtz, R. H. Modulation of neuronal activity in superior colliculus by changes in target probability. *J. Neurosci.* **18**, 7519–7534 (1998).
15. McPeek, R. M. & Keller, E. L. Deficits in saccade target selection after inactivation of superior colliculus. *Nat. Neurosci.* **7**, 757–763 (2004).
16. Carello, C. D. & Krauzlis, R. J. Manipulating intent: evidence for a causal role of the superior colliculus in target selection. *Neuron* **43**, 575–583 (2004).
17. Horwitz, G. D. & Newsome, W. T. Separate signals for target selection and movement specification in the superior colliculus. *Science* **284**, 1158–1161 (1999).
18. Horwitz, G. D. & Newsome, W. T. Target selection for saccadic eye movements: prelude activity in the superior colliculus during a direction- discrimination task. *J. Neurophysiol.* **86**, 2543–2558 (2001).
19. Ratcliff, R., Cherian, A. & Segraves, M. A comparison of macaque behavior and superior colliculus neuronal activity to predictions from models of two-choice decisions. *J. Neurophysiol.* **90**, 1392–1407 (2003).
20. Horwitz, G. D., Batista, A. P. & Newsome, W. T. Representation of an abstract perceptual decision in macaque superior colliculus. *J. Neurophysiol.* **91**, 2281–2296 (2004).
21. Crapse, T. B., Lau, H. & Basso, M. A. A role for the superior colliculus in decision criteria. *Neuron* **97**, 181–194.e6 (2018).
22. Jun, E. J. et al. Causal role for the primate superior colliculus in the computation of evidence for perceptual decisions. *Nat. Neurosci.* **24**, 1121–1131 (2021).
23. Stine, G. M., Trautmann, E. M., Jeurissen, D. & Shadlen, M. N. A neural mechanism for terminating decisions. *Neuron* **111**, 2601–2613.e5 (2023).
24. Ignashchenkova, A., Dicke, P. W., Haarmeier, T. & Thier, P. Neuron-specific contribution of the superior colliculus to overt and covert shifts of attention. *Nat. Neurosci.* **7**, 56–64 (2004).
25. Cavanaugh, J. & Wurtz, R. H. Subcortical modulation of attention counters change blindness. *J. Neurosci.* **24**, 11236–11243 (2004).
26. Müller, J. R., Philiastides, M. G. & Newsome, W. T. Microstimulation of the superior colliculus focuses attention without moving the eyes. *Proc. Natl Acad. Sci. USA* **102**, 524–529 (2005).
27. Cavanaugh, J., Alvarez, B. D. & Wurtz, R. H. Enhanced performance with brain stimulation: attentional shift or visual cue? *J. Neurosci.* **26**, 11347–11358 (2006).
28. Lovejoy, L. P. & Krauzlis, R. J. Inactivation of primate superior colliculus impairs covert selection of signals for perceptual judgments. *Nat. Neurosci.* **13**, 261–266 (2010).
29. Zénon, A. & Krauzlis, R. J. Attention deficits without cortical neuronal deficits. *Nature* **489**, 434–437 (2012).
30. Krauzlis, R. J., Lovejoy, L. P. & Zénon, A. Superior colliculus and visual spatial attention. *Annu. Rev. Neurosci.* **36**, 165–182 (2013).
31. Fries, W. Cortical projections to the superior colliculus in the macaque monkey: a retrograde study using horseradish peroxidase. *J. Comp. Neurol.* **230**, 55–76 (1984).
32. Lynch, J. C., Graybiel, A. M. & Lobeck, L. J. The differential projection of two cytoarchitectonic subregions of the inferior parietal lobule of macaque upon the deep layers of the superior colliculus. *J. Comp. Neurol.* **235**, 241–254 (1985).
33. Asanuma, C., Andersen, R. A. & Cowan, W. M. The thalamic relations of the caudal inferior parietal lobule and the lateral prefrontal cortex in monkeys: divergent cortical projections from cell clusters in the medial pulvinar nucleus. *J. Comp. Neurol.* **241**, 357–381 (1985).
34. Andersen, R. A., Asanuma, C., Essick, G. & Siegel, R. M. Corticocortical connections of anatomically and physiologically defined subdivisions within the inferior parietal lobule. *J. Comp. Neurol.* **296**, 65–113 (1990).
35. Paré, M. & Wurtz, R. H. Monkey posterior parietal cortex neurons antidromically activated from superior colliculus. *J. Neurophysiol.* **78**, 3493–3497 (1997).
36. Clower, D. M., West, R. A., Lynch, J. C. & Strick, P. L. The inferior parietal lobule is the target of output from the superior colliculus, hippocampus, and cerebellum. *J. Neurosci.* **21**, 6283–6291 (2001).
37. Zhou, Y. & Freedman, D. J. Posterior parietal cortex plays a causal role in perceptual and categorical decisions. *Science* **365**, 180–185 (2019).
38. Zhou, Y., Zhu, O. & Freedman, D. J. Posterior parietal cortex plays a causal role in abstract memory-based visual categorical decisions. *J. Neurosci.* **43**, 4315–4328 (2023).
39. Swaminathan, S. K. & Freedman, D. J. Preferential encoding of visual categories in parietal cortex compared to prefrontal cortex. *Nat. Neurosci.* **15**, 315–320 (2012).

40. Swaminathan, S. K., Masse, N. Y. & Freedman, D. J. A comparison of lateral and medial intraparietal areas during a visual categorization task. *J. Neurosci.* **33**, 13157–13170 (2013).
41. Sarma, A., Masse, N. Y., Wang, X.-J. & Freedman, D. J. Task-specific versus generalized mnemonic representations in parietal and prefrontal cortices. *Nat. Neurosci.* **19**, 143–149 (2016).
42. Zhou, Y., Mohan, K. & Freedman, D. J. Abstract encoding of categorical decisions in medial superior temporal and lateral intraparietal cortices. *J. Neurosci.* **42**, 9069–9081 (2022).
43. Freedman, D. J. & Assad, J. A. Experience-dependent representation of visual categories in parietal cortex. *Nature* **443**, 85–88 (2006).
44. Rishel, C. A., Huang, G. & Freedman, D. J. Independent category and spatial encoding in parietal cortex. *Neuron* **77**, 969–979 (2013).
45. Mohan, K., Zhu, O. & Freedman, D. J. Interaction between neuronal encoding and population dynamics during categorization task switching in parietal cortex. *Neuron* **109**, 700–712.e4 (2021).
46. Dotson, N. M., Hoffman, S. J., Goodell, B. & Gray, C. M. Feature-based visual short-term memory is widely distributed and hierarchically organized. *Neuron* **99**, 215–226.e4 (2018).
47. Musall, S., Kaufman, M. T., Juavinett, A. L., Gluf, S. & Churchland, A. K. Single-trial neural dynamics are dominated by richly varied movements. *Nat. Neurosci.* **22**, 1677–1686 (2019).
48. Mante, V., Sussillo, D., Shenoy, K. V. & Newsome, W. T. Context-dependent computation by recurrent dynamics in prefrontal cortex. *Nature* **503**, 78–84 (2013).
49. Elsayed, G. F., Lara, A. H., Kaufman, M. T., Churchland, M. M. & Cunningham, J. P. Reorganization between preparatory and movement population responses in motor cortex. *Nat. Commun.* **7**, 13239 (2016).
50. Zhong, L. et al. Causal contributions of parietal cortex to perceptual decision-making during stimulus categorization. *Nat. Neurosci.* **22**, 963–973 (2019).
51. Duan, C. A. et al. Collicular circuits for flexible sensorimotor routing. *Nat. Neurosci.* **24**, 1110–1120 (2021).
52. Duan, C. A., Erlich, J. C. & Brody, C. D. Requirement of prefrontal and midbrain regions for rapid executive control of behavior in the rat. *Neuron* **86**, 1491–1503 (2015).
53. Felsen, G. & Mainen, Z. F. Neural substrates of sensory-guided locomotor decisions in the rat superior colliculus. *Neuron* **60**, 137–148 (2008).
54. Ferrera, V. P., Yanike, M. & Cassanello, C. Frontal eye field neurons signal changes in decision criteria. *Nat. Neurosci.* **12**, 1458–1462 (2009).
55. Born, R. T. & Bradley, D. C. Structure and function of visual area MT. *Annu. Rev. Neurosci.* **28**, 157–189 (2005).
56. Fitzgerald, J. K., Freedman, D. J. & Assad, J. A. Generalized associative representations in parietal cortex. *Nat. Neurosci.* **14**, 1075–1079 (2011).
57. Kawai, R. et al. Motor cortex is required for learning but not for executing a motor skill. *Neuron* **86**, 800–812 (2015).
58. Mysore, S. P. & Knudsen, E. I. Flexible categorization of relative stimulus strength by the optic tectum. *J. Neurosci.* **31**, 7745–7752 (2011).

Methods

Subjects

Two adult (13–15 yr old) male rhesus macaques (*Macaca mulatta*) participated in the experiment (Monkey N: ~12 kg, Monkey S: ~13 kg). All procedures were in accordance with the University of Chicago Institutional Animal Care and Use Committee and the National Institutes of Health guidelines and policies.

Behavioral tasks

For the behavioral tasks described below, the monkeys were head restrained and seated in a primate chair inserted inside an isolation box (Crist Instrument), facing a 60.96-cm LCD monitor on which stimuli were presented (1,920 × 1,080 resolution, refresh rate 60 Hz, 57-cm viewing distance). Reward delivery, stimulus presentation, behavioral signals and task events were controlled by MonkeyLogic 2.0 software[59], running under MATLAB 2015–2022 on a Windows-based PC. Gaze position was measured with an optical eye tracker (Eyelink 1000; SR Research) with a 1.0-kHz sample rate. For both tasks, monkeys initiated trials by holding a manual touch bar.

DMC task. We trained monkeys to perform a DMC task in which they grouped 12 directions of dot-motion stimuli into two categories based on two orthogonal boundaries, such that motion directions that are 180° apart belong to the same category. Motion directions were separated into quadrants with three directions per quadrant, and stimuli within the same quadrant were 22.5° apart and near-boundary directions were 22.5° away from the boundary. We used the same stimulus parameters (for example, stimulus size, contrast, speed and so on) for both animals and for SC and LIP recordings. The stimuli were 6°-diameter circular patches of white dots moving at a speed of 10° s^{-1} with 100% coherence, presented at 6.5–7.5° eccentricity in the contralateral visual field. Animals were required to fixate within a 2.5–3.5° radius circular window.

MGS task. We used an MGS task[60] to identify visual and motor receptive fields of LIP and SC neurons (Supplementary Fig. 8). At the start of a trial, monkeys had to maintain fixation on a central ~0.25° white spot for 500 ms, after which an ~0.5° white square target briefly appeared for 300 ms at one of eight peripheral locations (equally spaced and concentric at 6.5° eccentricity). The target presentation was followed by a 1,000-ms delay period, after which the fixation cue disappeared and monkeys had to saccade to the remembered location of the visual target presented earlier in the trial.

Passive viewing of motion stimuli. On DMC recording sessions, monkeys also performed interleaved blocks of a passive viewing paradigm in which they were shown the same motion stimuli used in the DMC task (and presented at the same peripheral location). At the start of a trial, a blue fixation circle appeared to indicate a passive viewing trial to monkeys (as opposed to a white fixation circle for the DMC task). Monkeys had to maintain gaze fixation on this central cue for 500 ms, after which 3–5 motion stimuli appeared in succession for 400 ms each and separated by 200 ms. Monkeys received a fluid reward at the end of the trial for maintaining gaze fixation on the central cue.

Surgical procedures and electrophysiological recordings

We followed procedures that were described in detail in previous studies from our group[37,42,45]. Monkeys were implanted with a titanium headpost and a single recording chamber positioned over LIP and SC. Stereotaxic coordinates for chamber placement were determined from magnetic resonance imaging scans obtained before implantation of recording chambers. LIP and SC recordings were conducted in separate sessions, typically using 16- and 24-channel linear Plexon V-probes (in which channels span 1.5–2.0 mm of tissue), a dura-piercing guide tube, a Plexon Omniplex acquisition system and a NAN microdrive system (NAN Instruments). A small subset of recording sessions from one monkey were conducted using single epoxy-insulated tungsten electrodes (FHC). We used anatomical landmarks and responses during the MGS task to guide recordings. For SC recordings, we primarily targeted neurons in superficial and intermediate layers, although we also recorded neurons in deep layers as well due to the ~2-mm span of recording channels on our probes. Neurophysiological signals were amplified, digitized and stored for offline spike sorting (Plexon) to verify the quality and stability of neuronal isolation.

SC inactivation

We infused muscimol, a $GABA_A$ agonist, to unilaterally inactivate the SC. Muscimol was dissolved in PBS to a concentration of 5 μg $μl^{-1}$. We built a microfluidic injectrode system to deliver small amounts of the drug or saline (muscimol: 0.25–0.33 μl; saline: 0.25–0.5 μl; Supplementary Table 1) using the protocol developed previously[61]. To ensure that we precisely injected the drug into superficial and intermediate layers of the SC, we used a custom 16-channel Plexon S-probe with a fluid delivery channel that allowed us to monitor neural activity during probe lowering and before injection. Before drug injection on each session, monkeys first completed a control behavioral session in which they performed at least 200 correct trials of the DMC task and at least 100 correct trials of the MGS task (Monkey N) or the VGS task (Monkey S). After monkeys completed the control behavioral session, we infused the drug and waited 15–25 min to begin the post-treatment behavioral session. To verify success of SC inactivation, we compared saccade metrics (peak saccade velocity) during the MGS/VGS tasks during the control and post-treatment trials. We analyzed data from 12 muscimol injection sessions (Monkey N: 6 sessions, Monkey S: 6 sessions) and six control saline injection sessions (Monkey N: 2 sessions, Monkey S: 4 sessions). Supplementary Table 1 provides information for each injection session, including muscimol and saline concentration, injection volume and number of completed DMC trials.

LIP inactivation

We compared behavioral results from the SC inactivation experiments described above with data from a previous study from our group[38] that investigated the effect of LIP inactivation (using muscimol) on DMC task performance. The LIP inactivation experiment was performed in a different pair of monkeys (Monkey Q and Monkey M) than the ones used for the LIP/SC electrophysiological recordings and SC inactivation experiments reported here. The procedure used to infuse muscimol to reversibly inactivate the LIP is described in detail in ref. 38. We will highlight the differences between the SC inactivation procedure described above and the LIP inactivation procedure: (1) the LIP inactivation experiments used a higher muscimol concentration than the SC inactivation experiments (LIP: 8 μg $μl^{-1}$, SC: 5 μg $μl^{-1}$); (2) in the LIP inactivation experiments, a much larger volume of muscimol was infused than in the SC inactivation experiments (LIP: 6–9 μl; SC: 0.25–0.33 μl); and (3) the motion DMC tasks had a different category boundary for the LIP versus SC inactivation experiments (the task used for the LIP inactivation experiment had a single 45° boundary separating motion directions into two categories, rather than the two orthogonal boundaries used in the SC inactivation experiment).

Behavioral inclusion criteria

For electrophysiological recordings and inactivation experiments, we included sessions in which behavioral performance on each category for the DMC task was at least 75% (criterion applied only to control blocks for the inactivation experiments). We excluded six LIP recording sessions (four in Monkey N and two in Monkey S) from analyses due to poor behavioral performance. For the inactivation experiments, we excluded two sessions in Monkey S (one saline injection session with 66% accuracy for category 2 during the control block, and one

muscimol injection session with 53% accuracy for category 2 during the control block).

For DMC analyses, we included well-isolated neurons for which we had data recorded during at least five correct trials for each sample direction. We analyzed spiking data during the DMC task from 555 LIP neurons recorded over 49 recording sessions (Monkey N: *n* neurons = 228, *n* sessions = 36; Monkey S: *n* neurons = 327, *n* sessions = 13) and 605 SC neurons recorded over 38 recording sessions (Monkey N: *n* neurons = 362, *n* sessions = 26; Monkey S: *n* neurons = 243, *n* sessions = 12). We collected and analyzed spiking activity during the MGS task in a subset of 424 SC neurons (Monkey N: *n* = 259, Monkey S: *n* = 165) for which we recorded data from least two correct trials for each MGS condition.

Data analysis

Analyses were performed in Python (v.3.7.3) or MATLAB (v.R2019a–R2023b). Behavioral analyses for the DMC task (including those for inactivation) were performed on all completed trials (that is, correct trials, misses on Match trials and false alarms on Nonmatch trials). Unless otherwise specified, all neural analyses for the DMC task were performed only on correct trials. Behavioral and neural analyses for the MGS/VGS tasks were performed only on correct (completed) trials. All *P* values are two-tailed unless otherwise specified. For neural analyses, spike trains for each neuron were smoothed using a Gaussian kernel (σ = 25 ms). Eye tracker gaze position data were low-pass filtered to reduce noise using a second-order Butterworth filter with a 70-Hz cutoff.

Behavioral performance

To compare differences in mean behavioral accuracy (across all sample directions) between LIP and SC recording sessions in each monkey (Extended Data Fig. 1a), we used a permutation test in which we randomly permuted mean accuracy values between the two brain areas (while preserving the number of sessions per area). We repeated this procedure for 5,000 unique iterations to generate a null distribution of accuracy differences. To compare differences in behavioral performance on match trials in which the sample and test stimuli were in the same versus opposite quadrants, we computed the difference in mean accuracy for same versus opposite quadrant match trials for each session and used a permutation test (with 5,000 iterations) to randomly permute the per-session accuracy values between the two conditions.

Quantifying single-neuron category tuning

We quantified the strength, reliability and time course of single-neuron category tuning using an rCTI[44]. For each neuron, we applied ROC analysis to distributions of trial-by-trial firing rates and compared area under the ROC curve (AUC) values for eight pairs of sample motion directions that are in the same category (Within-Category; WC) and eight pairs of directions that are in different categories (Between-Category; BC). To ensure equalized angle differences between WC and BC pairs (and thus minimize the influence of direction tuning on rCTI), the WC and BC groups each included four direction pairs spaced 45° apart and four direction pairs spaced 135° apart (Extended Data Fig. 2). We quantified rCTI at each timepoint as the mean rectified WC AUC subtracted from the mean rectified BC AUC:

$$\mathrm{rCTI} = \frac{1}{8}\sum_{p=1}^{8} 0.5 + \left|0.5 - \mathrm{AUC}\left(\mathrm{BC}_{p1}, \mathrm{BC}_{p2}\right)\right|$$

$$-\frac{1}{8}\sum_{p=1}^{8} 0.5 + \left|0.5 - \mathrm{AUC}\left(\mathrm{WC}_{p1}, \mathrm{WC}_{p2}\right)\right|$$

where BC_{p1} and BC_{p2} are the two directions in the *p*th BC pair (*p*), and WC_{p1} and WC_{p2} are the two directions in the *p*th WC pair.

We applied the rCTI analysis to smoothed spike trains (see above) across 5-ms time steps in the trial. To generate the error shading shown in Fig. 2c,d, we calculated rCTI for each neuron over 500 bootstraps using ten trials per sample motion direction (sampled with replacement from a pool of 50% of trials for each bootstrap). We generated null distributions of rCTI values for each neuron using a bootstrap analysis (repeated 5,000 times) in which we randomly assigned (with replacement) eight direction pairs (four 45°-spaced and four 135°-spaced pairs) to each of the shuffled BC and WC groups (Extended Data Fig. 2). In this procedure, we reshuffled the labels (BC versus WC) assigned to each pair of directions, such that each shuffled group contained four 45°-apart direction pairs and four 135°-apart direction pairs. We defined category-tuned 'runs' as time bins at which rCTI values significantly exceed the null distribution for a minimum of five consecutive analysis time bins (25 ms). We considered neurons to be category-tuned if they were classified as task-responsive and had at least one significant run, and defined latency of category selectivity for each category-tuned neuron as the first time bin of the earliest significant run.

To test for significant above-chance mean rCTI in each brain area (as shown in Fig. 2f), we used a permutation procedure in which we computed a null mean rCTI across neurons for each WC/BC-label-shuffling iteration. To test for a significant difference between brain areas in the onset time of category selectivity for mean rCTI, we compared the observed between-area latency difference with a null distribution of latency differences. For each of 5,000 iterations, we randomly permuted neurons between the two brain areas (while preserving the number of neurons in each area) and we computed the difference in latency of category selectivity onset in the two shuffled groups. To test for differences in onset time of category selectivity between Vis and Vis-other SC neurons, we used a similar procedure in which we randomly permuted neurons between the two groups instead of between brain areas.

SVM analyses

We used SVM classifiers (with a linear kernel) to quantify the strength and timing of sample stimulus category encoding in populations of LIP and SC neurons. To quantify category encoding in a direction-independent manner, we constructed cross-quadrant classifiers for which training sets consisted of trials in which the sample motion directions were from two of the four quadrants (one from each category), and testing sets consisted of sample motion direction trials from the other two quadrants (Fig. 2g). The training and testing quadrants were randomly chosen on each iteration. The analysis was applied in 5-ms steps across time in the trial and repeated for 200 iterations. For each neuron, we included 15 trials from each of six sample motion directions for training (as described above) and 15 trials from each of the remaining six sample motion directions for testing. To reduce the biases in classifier performance across brain areas due to an unequal number of neurons, for each iteration of the analysis, we randomly selected *N* neurons for inclusion, where *N* is the number of neurons in the brain area with the lower number of neurons. We generated null distributions of decoder performance values at each time using a permutation procedure (repeated 5,000 times) in which we shuffled the sample direction label assigned to each trial.

We also used linear SVM classifiers to decode sample direction from LIP and SC population activity. To quantify the amount of direction encoding in a category-independent manner, the training/validation sets for each iteration of the classifier only included data from one of the two categories. The classifiers were trained on 48 trials (eight trials from each of the six directions from one of the two categories, randomly chosen) and validated on 12 held-out trials (two trials from each of the six motion directions). This analysis was applied in 5-ms steps across the trial and repeated for 200 iterations.

Mean matching procedure

We controlled for the possibility that differences in mean firing rates between LIP and SC neurons could interfere in our measures of neuronal

category selectivity strength or latency by performing a mean matching procedure on the raw data before performing some of the rCTI analyses (where indicated in Results). For each 20-ms time window in sequence from the fixation period through first test period, we computed the mean spike count across all neurons in LIP and in SC. For the area that had the higher mean (usually SC, which had higher average rates overall), spikes were removed from that area at random (across neurons and trials) until the means were matched at that time step.

Identifying task-responsive neurons

To identify neurons that are task-responsive during the DMC task, we used a bin- and parameter-free statistical test (ZETaPY) to detect any consistent time-locked modulations in firing rate for each neuron[62]. In brief, this analysis consists of the following steps (applied separately for each sample direction): (1) aligning the spike trains for all correct trials to the onset of the sample stimulus, (2) stacking these spike trains to create a single vector of spikes relative to sample onset, (3) calculating the cumulative distribution of spikes over trial time using this spike vector and (4) comparing this cumulative distribution with a linear baseline (which represents an unvarying firing rate over time), producing a deviation value for each timepoint. To generate a null distribution of 5,000 deviation-from-baseline values, we shuffled the spike trains in each trial to destroy any time-locked activity patterns across trials while preserving the total number of spikes, and then computed the maximum deviation (across time) for these shuffled data. For this analysis, we included data for each trial from 100 ms before sample stimulus onset until the end of the first test stimulus epoch. We also computed the peak mean firing across time (in the period from the beginning of the sample epoch until the end of the first test epoch) for each sample direction. We classified each neuron as task-responsive if it satisfied the following two criteria: (1) if it showed a significant modulation in firing rate (that is, had significantly elevated deviation-from-linear-baseline values) at any timepoint from the start of the sample epoch until the end of the test epoch; and (2) if its maximum peak mean firing rate (across sample directions) was at least 3.0 spikes per s. In LIP, 506 of 555 neurons (91.2%) were task-responsive (Monkey N: 210 of 228, 92.1%; Monkey S: 296 of 327, 90.5%), and in SC, 493 of 605 neurons (81.5%) were task-responsive (Monkey N: 296 of 362, 81.8%; Monkey S: 197 of 243, 84.4%).

Identifying direction-tuned neurons during the DMC task

To identify neurons that are significantly direction-tuned during the sample epoch of the DMC task, we computed a direction tuning index (DTI) for each neuron using the circular variance method introduced previously[63]. We calculated the neurons' mean firing rate for each sample stimulus direction in a direction vector space, and quantified DTI as the normalized length of the sum of these vectors:

$$\mathrm{DTI} = \left| \frac{\sum_{k=1}^{12} f(\theta_k) e^{i\theta_k}}{\sum_{k=1}^{12} f(\theta_k)} \right|$$

where $f(\theta_k)$ is a neuron's mean firing rate for direction θ_k.

To test for significant direction tuning, we compared the true DTI with a distribution of 5,000 null DTIs generated by randomly shuffling the direction labels assigned to each mean firing rate. We applied this analysis to firing rates in three nonoverlapping 200-ms windows from 0 to +600 ms relative to sample stimulus onset. We classified neurons as direction-tuned if they showed significant direction tuning during at least one of the three time windows and if they were identified as responsive during the DMC task (see above). In LIP, 156 of 555 neurons (28.1%) were significantly direction-tuned (Monkey N: 78 of 228, 34.2%; Monkey S: 78 of 327, 23.9%), and in SC, 107 of 605 neurons (17.7%) were significantly direction-tuned (Monkey N: 52 of 362, 14.4%; Monkey S: 55 of 243, 22.6%).

MGS task analyses

Identifying visually responsive neurons. We analyzed neuronal activity during the MGS task to characterize the visual and motor response fields of SC neurons. For each neuron, we determined whether the DMC stimulus was presented in its visual receptive field by identifying the MGS condition ($\mathrm{MGS}_{\mathrm{DMCloc}}$) whose location overlapped with the DMC stimulus location on that session. We then determined whether the neuron was significantly modulated during the MGS visual epoch for that condition. For each of the eight MGS conditions, we computed the mean firing rate (per trial) for each nonoverlapping 25-ms bin from 0 ms to +400 ms relative to stimulus onset. We used the Kruskal–Wallis *H*-test to compare the firing rate distributions across these windows and compared the resulting *H*-statistic with a distribution of 5,000 null *H*-statistics. To generate the null *H* distribution, we shuffled the neuron's time-varying firing rates (from 0 to +400 ms relative to stimulus onset) for each trial, calculated the mean firing in nonoverlapping 25-ms windows for these permuted trials and computed a shuffled *H*-statistic. In addition, we applied the ZETaPY procedure (described above) to detect any consistent time-locked modulations in firing rate for each condition (applied from −100 ms to +400 ms relative to stimulus onset). Neurons were classified as 'Vis' neurons if they were significantly modulated across the visual stimulus period based on the *H*-test or ZETaPY test for the $\mathrm{MGS}_{\mathrm{DMCloc}}$ condition and if their maximum firing rate was above 3.0 spikes per s. Neurons were classified as 'Vis-other' if they were significantly modulated across the visual stimulus period for another MGS condition (and if their maximum firing rate was above 3.0 spikes per s). Neurons were classified as 'Non-vis' if they were not significantly modulated across the visual period for any of the MGS conditions, or if their maximum firing rate across analysis windows and conditions was below 3.0 spikes per s. To minimize inclusion bias between the Vis group and the other two groups, *P* values for the seven non-$\mathrm{MGS}_{\mathrm{DMCloc}}$ conditions were Bonferroni-corrected. In total, 127 neurons (30.0%) were classified as Vis neurons (Monkey N: 90 (34.7%), Monkey S: 37 (22.4%)), 167 (39.4%) as Vis-other neurons (Monkey N: 90 (34.7%), Monkey S: 77 (46.7%)) and 130 (30.7%) as Non-vis neurons (Monkey N: 79 (30.5%), Monkey S: 51 (30.9%)).

Identifying saccade-modulated neurons. We analyzed activity of SC neurons during the saccade period of the MGS task (−200 ms to +50 ms relative to saccade onset) to identify neurons that are significantly modulated by saccade direction. For each neuron, we computed its mean firing rate across the saccade period window for each trial. We used the Kruskal–Wallis *H*-test to compare the neuron's firing rate distributions across the eight MGS conditions, and compared the resulting *H*-statistic with a distribution of 5,000 null *H*-statistics generated by shuffling condition labels among trials. In total, 124 of 424 neurons (29.2%) were significantly modulated by saccade direction (Monkey N: 80 of 259 (30.9%), Monkey S: 44 of 165 (26.7%)).

Quantifying contribution of stimulus category versus eye position to neuronal firing rates

We constructed linear encoding models[47] to quantify how much firing rates of individual neurons (across trials and time within trials) are modulated by stimulus category versus eye position. The linear models contained regressors related to stimulus category and microsaccade parameters. For the category regressors, we constructed a binary vector containing a pulse at the time of the sample stimulus onset, and created copies of this vector shifted in time by 1 ms for every point until the end of the trial. The microsaccade regressors included two analog regressors: horizontal and vertical eye velocity at each timepoint throughout the trial, shifted in time by −50 ms relative to neural activity to account for lag between neural activity and saccades. We also included two types of saccade event kernel regressors: (1) a binary vector containing a pulse at every timepoint at which a microsaccade occurred; and (2) a vector containing microsaccade direction at every

timepoint at which a microsaccade occurred and zeros at every other timepoint. We created time-shifted copies of the binary saccade vector and saccade direction vector, spanning from −500 ms until +100 ms (relative to saccade onset) in 10-ms steps. The design matrix of the full model included all of the category and saccade regressors. We also built reduced models that contained shuffled saccade regressors and unshuffled category regressors, or shuffled category regressors and unshuffled saccade regressors. For each neuron, we fit the models using ridge regression (with L2 regularization and tenfold cross-validation) and computed an R^2 for the full model and each of the reduced models. To quantify how well category or saccade regressors predict neural activity in each neuron, we computed the change in cross-validated R^2 from the full model to each reduced model. A large (negative) change in R^2 indicates a strong contribution of the excluded variables.

Subspace alignment analysis

We used a subspace alignment analysis introduced in ref. 49 to quantify the degree of alignment between neural activity in the SC during the MGS and DMC tasks. For this analysis, we constructed matrices D and M of neural activity during the DMC and MGS tasks, respectively. D and M were size N by $c \times t$, where N is the number of neurons, c the number of conditions (12 for DMC and 8 for MGS) and t is the number of timepoints per condition. Each row of D and M contains the concatenated mean firing rates (per condition and across timepoints) of one neuron. We normalized the firing rates of each neuron by its range (across all included DMC and MGS conditions and timepoints) plus a constant, chosen as 5 spikes per s. We then performed PC analysis on the matrix D to obtain the top 12 DMC PCs, and on matrix M to obtain the top 12 MGS PCs. We then projected the DMC activity D onto both the DMC and MGS PCs and calculated the sum of the percentage of variance explained (relative to total variance of D) for each of the projections. We quantified the AI between the two subspaces as the ratio of these two sums. The logic behind this analysis is that if the DMC and MGS subspaces are approximately orthogonal, the projection of D onto the MGS PCs will capture minimal D variance. AI ranges between 0 (indicating perfect orthogonality between two subspaces) and 1 (indicating perfect alignment).

To determine whether measured AI values are more (or less) misaligned than expected by chance, we calculated the alignment between pairs of random subspaces sampled from the full covariance structure of the data to generate a null distribution of alignment values[49]. To create the random subspaces, we first computed the covariance matrix C from the concatenated D and M matrices, and obtained the left singular vectors ($\mathbf{U}$) and singular values (s) of C using singular value decomposition. For each of 5,000 iterations per comparison, we computed the AI between two random subspaces (υ_{rand}). We sampled each random subspace υ_{rand} as follows:

$$\upsilon_{\text{rand}} = \text{orth}\left(\frac{\mathbf{U}\sqrt{s}\upsilon}{\|\mathbf{U}\sqrt{s}\upsilon\|_2}\right)$$

where υ is an $N \times 12$ matrix in which each element is drawn from a normal distribution with mean 0 and variance 1, and orth(X) returns the orthonormal basis of X defined by its left singular values.

For the main alignment analysis (shown in Fig. 3c–e), we included DMC task data from 150–350 ms after sample stimulus onset (during stimulus presentation) and MGS task data from 200m s before saccade onset until saccade onset. Data for both tasks were sampled in 10-ms steps.

SC inactivation analyses

To verify the efficacy of SC inactivation, we quantified the difference in peak saccade velocity for saccades made toward the inactivated hemifield during the MGS/VGS task between the control and post-treatment blocks. For each trial, we computed the maximum eye gaze velocity from 200 ms before go cue onset until successful target fixation initiation. We excluded one trial for Monkey N (session 2, muscimol treatment, upper-center condition) in which we could not accurately quantify peak saccade velocity because the monkey blinked during the response period. For each session, we combined trials from the three conditions in which the target was in the inactivated hemifield ('Contralateral'), and the three conditions in which the target was out of the inactivated hemifield ('Ipsilateral'). We tested for significant differences in mean peak saccade velocity between the control and treatment blocks for Contralateral and Ipsilateral trials on each session using a bootstrap test with 5,000 iterations (Supplementary Table 2). We also tested for significant differences in mean peak saccade velocity between control and treatment blocks for Contralateral trials pooled across all muscimol sessions and pooled across all saline sessions, as shown in Fig. 4c. For the muscimol sessions, this analysis included 270 (470) control (treatment) trials in Monkey N and 320 (376) control (treatment) trials in Monkey S, and for saline sessions included 72 (103) control (treatment) trials in Monkey N and 207 (215) control (treatment) trials in Monkey S.

We used a two-tailed Fisher exact test to quantify differences in behavioral performance on the DMC task between control and post-treatment blocks for each session. The statistics for the test are shown in Supplementary Table 3. We used a Wilcoxon rank-sum test to quantify differences in behavioral accuracy changes (from pre- to post-inactivation) between Category 1 and Category 2 trials (Extended Fig. 4a,b), Match and Nonmatch trials (Extended Fig. 4c,d) and Match trials in which Sample and Test stimuli are in the same versus opposite quadrants (Extended Fig. 4e,f).

Reporting summary

Further information on research design is available in the Nature Portfolio Reporting Summary linked to this article.

Data availability

Processed data for this manuscript are available via figshare at https://doi.org/10.6084/m9.figshare.25742958.v1 (ref. 64). Raw data are available upon request to the corresponding author.

Code availability

Data analysis code for accessing and analyzing data from this manuscript is available on GitHub at https://github.com/varya-p/visual_categorization_SC.

References

59. Asaad, W. F., Santhanam, N., McClellan, S. & Freedman, D. J. High-performance execution of psychophysical tasks with complex visual stimuli in MATLAB. *J. Neurophysiol.* **109**, 249–260 (2013).
60. Hikosaka, O. & Wurtz, R. H. Modification of saccadic eye movements by GABA-related substances. II. Effects of muscimol in monkey substantia nigra pars reticulata. *J. Neurophysiol.* **53**, 292–308 (1985).
61. Vanegas, M. I., Hubbard, K. R., Esfandyarpour, R. & Noudoost, B. Microinjectrode system for combined drug infusion and electrophysiology. *J. Vis. Exp.* **153**, e60365 (2019).
62. Montijn, J. S. et al. A parameter-free statistical test for neuronal responsiveness. *eLife* **10**, e71969 (2021).
63. Mazurek, M., Kager, M. & Van Hooser, S. D. Robust quantification of orientation selectivity and direction selectivity. *Front. Neural Circuits* **8**, 92 (2014).
64. Peysakhovich, B et al. Primate superior colliculus is causally engaged in abstract higher-order cognition. *figshare* https://doi.org/10.6084/m9.figshare.25742958.v1 (2024).

Acknowledgements

We thank the following individuals for helpful discussions and/or comments on an earlier version of this manuscript: C. Hauser, M. Kaufman, K. Latimer, J. MacLean, J. Maunsell, K. Mohan and Y. Zhou. We are grateful for expert technical assistance from

S. Chang, Y. Qiu and S. Zheng. We acknowledge expert animal care and veterinary support from the staff the University of Chicago Animal Resources Center. This work was supported by NIH grant no. R01EY019041, NIH grant no. U19NS107609, NIH NRSA grant no. 1F31MH124395 (B.P.), NIH NRSA grant no. F30EY033648 (O.Z.), NIH grant no. T32GM007281 (O.Z.), NIH NRSA grant no. F31 EY029155 (W.J.J.) and DOD Vannevar Bush Faculty Fellowship no. N000141912001 (D.J.F.). Figure 1e was adapted from 'Rhesus macaque monkey (brain, lateral)' by BioRender.com (https://www.biorender.com/icon/macaque-monkey-rhesus-macaca-mulatta-brain-lateral).

Author contributions

Project conceptualization was conducted by B.P. and D.J.F. Methodology was developed and conducted by B.P., S.M.T., A.A.S., S.L., O.Z., W.J.J., G.I., V.S., and D.J.F. Investigation was performed by B.P. Visualization was conducted by B.P., O.Z. and M.C.R. Funding acquisition was conducted by B.P., O.Z., W.J.J. and D.J.F. Overall project supervision was conducted by D.J.F. Writing of the original draft was done by B.P. and D.J.F, with review, editing and contributions by B.P., A.A.S., S.L., O.Z., G.I., W.J.J., M.C.R. and D.J.F.

Competing interests

The authors declare no competing interests.

Additional information

Extended data is available for this paper at https://doi.org/10.1038/s41593-024-01744-x.

Supplementary information The online version contains supplementary material available at https://doi.org/10.1038/s41593-024-01744-x.

Correspondence and requests for materials should be addressed to David J. Freedman.

Peer review information *Nature Neuroscience* thanks Steve Chang and the other, anonymous, reviewer(s) for their contribution to the peer review of this work.

https://doi.org/10.1038/s41593-024-01744-x

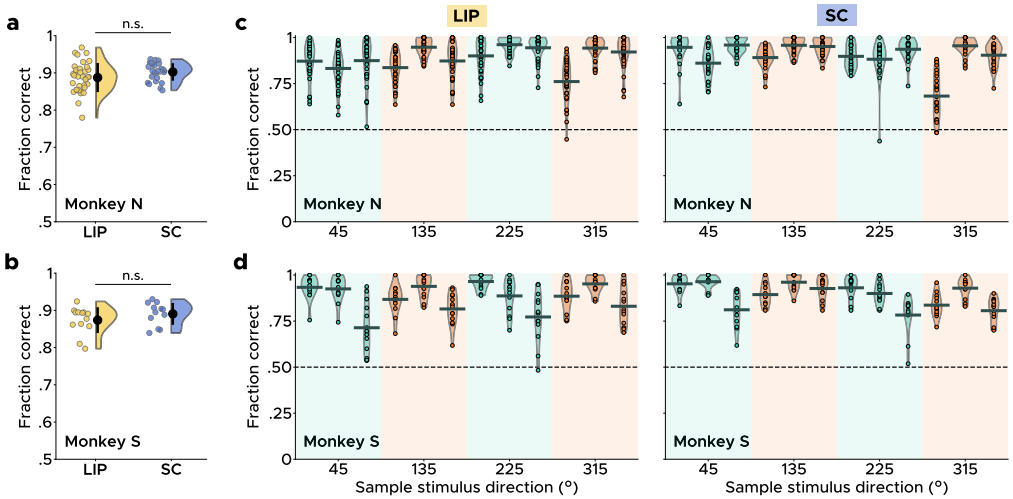

Extended Data Fig. 1 | No difference in behavioral performance between LIP and SC recording sessions. a, Distributions of overall session accuracy for LIP and SC recording sessions in Monkey N (LIP: n = 36 sessions; SC: n = 26 sessions). Black symbols indicate mean ± s.d. There was no difference in mean accuracy between brain areas (LIP: 88.8 ± 3.9%, SC: 90.3 ± 2.3%, P = 0.095, two-tailed permutation test). **b**, same as **a** but for Monkey S (LIP: n = 13 sessions, μ = 87.4 ± 3.5%; SC: n = 12 sessions, μ = 89.1 ± 2.9%, P = 0.234, two-tailed permutation test). **c**, Mean accuracy by sample direction for LIP (left) and SC (right) recording sessions. Horizontal bars indicate mean and plot bodies indicate range. **d**, same as **c** but for Monkey S.

https://doi.org/10.1038/s41593-024-01744-x

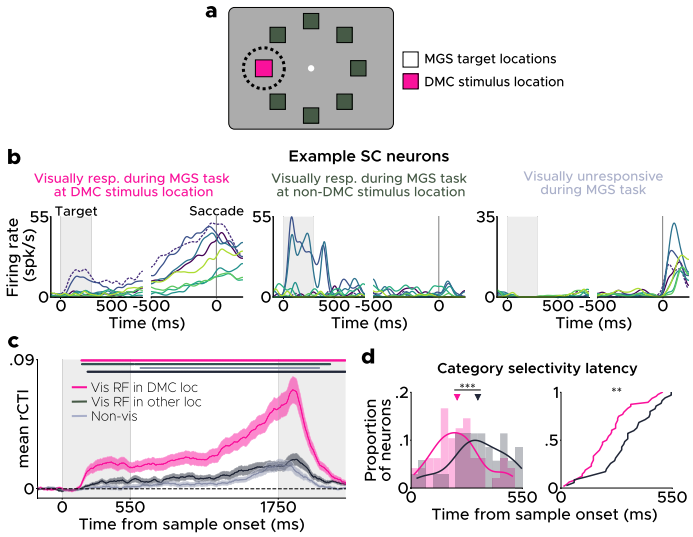

Extended Data Fig. 2 | Category tuning of visual and non-visual SC neurons. **a**, Schematic of the overlap between MGS target position and DMC stimulus position. Squares indicate the eight possible locations of the targets during the MGS task, and the dashed circle indicates the position of the DMC stimulus for an example session. **b**, Example PSTHs of SC neurons during the MGS task. Left: Neuron that is visually responsive during the MGS task to the target presented at the same location as the DMC task stimuli. Dashed line indicates MGS condition whose position matches the DMC stimulus. Center: Neuron that is visually unresponsive during the MGS task to the target presented at the same location as the DMC task stimuli, but is visually responsive to other MGS targets. Right: Neuron that is visually unresponsive to all stimuli during MGS task. **c**, Time course of mean rCTI across SC neurons that are visually responsive to stimuli at locations that overlap with the position of the DMC stimuli (pink), neurons that are visually unresponsive at DMC locations but visually responsive at other locations (dark grey), and neurons that are visually unresponsive (light grey). Shading indicates s.e.m. across neurons. Colored bars above plots indicate timepoints at which values significantly exceed chance. Black bars above panel indicate time points at which mean rCTI of Vis neurons is significantly higher than both Vis-other and Non-vis neurons ($P < 0.05$, two-tailed permutation tests). **d**, Latency of category selectivity for SC neurons that are category-tuned during the Sample epoch (0–550 ms from Sample onset) (Vis: n = 48 neurons, Vis-other: n = 35neurons). Left: Distribution of category selectivity latency. Triangular markers indicate median latency (Vis: 228 ± 75 ms, Vis-other: 330 ± 95; $P = 0.001$, two-tailed permutation test). Right: Empirical cumulative distribution functions of latency values in LIP and SC neurons (two-sample Kolmogorov-Smirnov test, $D = 0.407$, $P = 0.002$). (**$P < 0.005$), (***$P < 0.001$).

https://doi.org/10.1038/s41593-024-01744-x

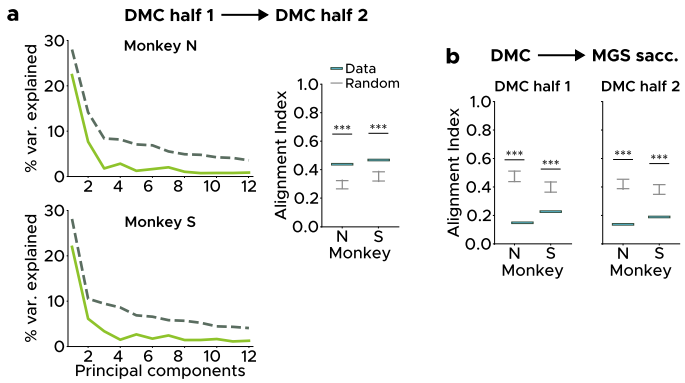

Extended Data Fig. 3 | Additional subspace alignment indices. a, Alignment between SC neural subspaces recorded during the first half and second half of the trials for each session. Data are significantly more aligned than chance (Monkey N: AI = 0.439, n = 235 neurons, $P < 0.001$; Monkey S: AI = 0.469, n = 150 neurons, $P < 0.001$, two-tailed randomization test). **b**, Left: SC neural subspaces during the first half of DMC trials and the MGS saccade period were significantly misaligned (Monkey N: AI = 0.151, n = 233 neurons, $P < 0.001$; Monkey S: AI = 0.229, n = 151 neurons, $P < 0.001$, two-tailed randomization test). Right: SC neural subspaces during the second half of DMC trials and the MGS saccade period were significantly misaligned (Monkey N: AI = 0.139, n = 235 neurons, $P < 0.001$; Monkey S: AI = 0.191, n = 151 neurons, $P < 0.001$). In **a** and **b**, alignment indices for the real data are indicated by horizontal blue lines and 95% confidence intervals of alignment indices between pairs of random vector projections from data (see Methods) are indicated in grey. (***$P < 0.001$).

https://doi.org/10.1038/s41593-024-01744-x

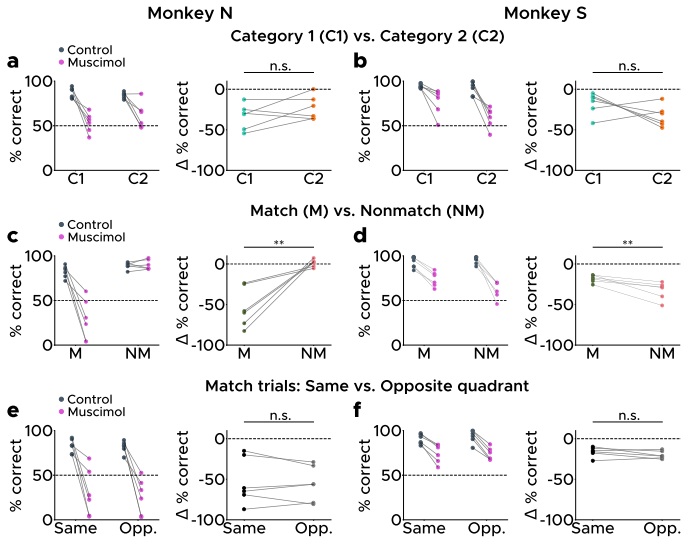

Extended Data Fig. 4 | Effect of SC inactivation on different trial types in the DMC task. a, Left: Behavioral performance (% correct) for Monkey N on Category 1 and Category 2 trials during control (grey) and inactivation (magenta) blocks. Right: Change in accuracy between control and inactivation blocks for Category 1 (cyan) and Category 2 (orange) trials. Negative values indicate decreased accuracy during inactivation blocks. Category 1 (median ± median absolute deviation %) = −29.9 ± 11.4, Category 2 = −26.5 ± 9.4, U = 13, P = 0.485, two-tailed Wilcoxon rank-sum test. **b**, Same as **a** but for Monkey S. Category 1 = −12.2 ± 5.6, Category 2 = −34.5 ± 7.7, U = 1, P = 0.065. **c**, Left: Behavioral performance (% correct) for Monkey N on Match and Nonmatch trials during control (grey) and inactivation (magenta) blocks. Right: Change in accuracy between control and inactivation blocks for Match (green) and Nonmatch (pink) trials. Match = −59.1 ± 18.8%, Nonmatch = 2.3 ± 2.9%, U = 0, P = 0.002, two-tailed Wilcoxon rank-sum test. **d**, Same as **c** but for Monkey S. Match = −17.6 ± 3.6, Nonmatch = −28.4 ± 4.6, U = 1, P = 0.004. **e**, Left: Behavioral performance (% correct) for Monkey N on Match trials in which Sample and Test stimuli are in the same vs. opposite quadrants. Right: Change in accuracy between control and inactivation blocks for same-quadrant (black) and opposite-quadrant (light grey) trials. Same quad. = −62.5 ± 15.2, Opposite quad. = −55.9 ± 22.8, U = 18, P = 0.936, two-tailed Wilcoxon rank-sum test. **f**, Same as **e** but for Monkey S. Same quad. = −15.2 ± 3.0, Opposite quad. = −21.1 ± 3.0, U = 25, P = 0.310, two-tailed Wilcoxon rank-sum test. For all comparisons, n = 6 control and 6 treatment blocks for each monkey.

nature portfolio

Corresponding author(s): David J. Freedman, dfreedman@uchicago.

Last updated by author(s): Apr 24, 2024

Reporting Summary

Nature Portfolio wishes to improve the reproducibility of the work that we publish. This form provides structure for consistency and transparency in reporting. For further information on Nature Portfolio policies, see our Editorial Policies and the Editorial Policy Checklist.

Statistics

For all statistical analyses, confirm that the following items are present in the figure legend, table legend, main text, or Methods section.

n/a	Confirmed
☐	☒ The exact sample size (*n*) for each experimental group/condition, given as a discrete number and unit of measurement
☐	☒ A statement on whether measurements were taken from distinct samples or whether the same sample was measured repeatedly
☐	☒ The statistical test(s) used AND whether they are one- or two-sided *Only common tests should be described solely by name; describe more complex techniques in the Methods section.*
☒	☐ A description of all covariates tested
☒	☐ A description of any assumptions or corrections, such as tests of normality and adjustment for multiple comparisons
☐	☒ A full description of the statistical parameters including central tendency (e.g. means) or other basic estimates (e.g. regression coefficient) AND variation (e.g. standard deviation) or associated estimates of uncertainty (e.g. confidence intervals)
☐	☒ For null hypothesis testing, the test statistic (e.g. *F*, *t*, *r*) with confidence intervals, effect sizes, degrees of freedom and *P* value noted *Give P values as exact values whenever suitable.*
☒	☐ For Bayesian analysis, information on the choice of priors and Markov chain Monte Carlo settings
☒	☐ For hierarchical and complex designs, identification of the appropriate level for tests and full reporting of outcomes
☒	☐ Estimates of effect sizes (e.g. Cohen's *d*, Pearson's *r*), indicating how they were calculated

Our web collection on statistics for biologists contains articles on many of the points above.

Software and code

Policy information about availability of computer code

Data collection	Neural data collection was conducted using Plexon Omniplex Software versions 2019-2023. Behavioral data collection was conducted using MATLAB Versions 2015-2022 and NIMH Monkeylogic Libraries version 2.
Data analysis	Analyses were performed in Python (version 3.7.3) or MATLAB (versions R2019a-R2023b).

For manuscripts utilizing custom algorithms or software that are central to the research but not yet described in published literature, software must be made available to editors and reviewers. We strongly encourage code deposition in a community repository (e.g. GitHub). See the Nature Portfolio guidelines for submitting code & software for further information.

Data

Policy information about availability of data

All manuscripts must include a data availability statement. This statement should provide the following information, where applicable:

- Accession codes, unique identifiers, or web links for publicly available datasets
- A description of any restrictions on data availability
- For clinical datasets or third party data, please ensure that the statement adheres to our policy

All neuronal and behavioral data along with code for processing the data will be made publicly available prior to publication via Figshare (figshare.com).

Research involving human participants, their data, or biological material

Policy information about studies with human participants or human data. See also policy information about sex, gender (identity/presentation), and sexual orientation and race, ethnicity and racism.

Reporting on sex and gender	N/A
Reporting on race, ethnicity, or other socially relevant groupings	N/A
Population characteristics	N/A
Recruitment	N/A
Ethics oversight	N/A

Note that full information on the approval of the study protocol must also be provided in the manuscript.

Field-specific reporting

Please select the one below that is the best fit for your research. If you are not sure, read the appropriate sections before making your selection.

☒ Life sciences ☐ Behavioural & social sciences ☐ Ecological, evolutionary & environmental sciences

For a reference copy of the document with all sections, see nature.com/documents/nr-reporting-summary-flat.pdf

Life sciences study design

All studies must disclose on these points even when the disclosure is negative.

Sample size	The sample size of the primary dataset is 555 LIP and 605 SC neurons recorded from two adult male rhesus macaques (Macaca mulatta). Using data from two rhesus monkeys is standard for neurophysiological studies in macaques (e.g., McGinty, VB & Lupkin, SM. [2023]. Behavioral read-out from population value signals in primate orbitofrontal cortex. Nat Neurosci 26, 2203–2212)
Data exclusions	For electrophysiological recordings and inactivation experiments, we included sessions in which behavioral performance on each category for the DMC task was at least 75% (criterion applied only to control blocks for the inactivation experiments). We excluded six LIP recording sessions (four in Monkey N and two in Monkey S) from analyses due to poor behavioral performance. For the inactivation experiments, we excluded two sessions in Monkey S (one saline injection session with 66% accuracy for category 2 during the control block, and one muscimol injection session with 53% accuracy for category 2 during the control block).
Replication	All analyses were conducted separately (and all results successfully replicated) in two subjects and reported as such in the manuscript.
Randomization	All comparisons were made within subjects and each subject was therefore their own control.
Blinding	N/A: Blinding was not relevant as no group allocation was done in this study

Reporting for specific materials, systems and methods

We require information from authors about some types of materials, experimental systems and methods used in many studies. Here, indicate whether each material, system or method listed is relevant to your study. If you are not sure if a list item applies to your research, read the appropriate section before selecting a response.

Materials & experimental systems

n/a	Involved in the study
☒	☐ Antibodies
☒	☐ Eukaryotic cell lines
☒	☐ Palaeontology and archaeology
☐	☒ Animals and other organisms
☒	☐ Clinical data
☒	☐ Dual use research of concern
☒	☐ Plants

Methods

n/a	Involved in the study
☒	☐ ChIP-seq
☒	☐ Flow cytometry
☒	☐ MRI-based neuroimaging

Animals and other research organisms

Policy information about studies involving animals; ARRIVE guidelines recommended for reporting animal research, and Sex and Gender in Research

Laboratory animals	Two adult (13-15 years old) male rhesus macaques (Macaca mulatta) participated in the experiment (Monkey N: ?12 kg, Monkey S: ? 13 kg).
Wild animals	No wild animals were used in this study
Reporting on sex	Two adult (13-15 years old) male rhesus macaques (Macaca mulatta) participated in the experiment (Monkey N: ?12 kg, Monkey S: ? 13 kg). Because of the small number of subjects and scarcity of animals, it is not always possible to have both sexes represented in a study or to statistically compare results between se
Field-collected samples	No field collected samples were used in the study.
Ethics oversight	All procedures were in accordance with the University of Chicago Institutional Animal Care and Use Committee and the National Institutes of Health guidelines and policies.

Note that full information on the approval of the study protocol must also be provided in the manuscript.